HHS Public Access

Author manuscript

Neuropharmacology. Author manuscript; available in PMC 2023 July 10.

Published in final edited form as:

Neuropharmacology. 2022 October 01; 217: 109204. doi:10.1016/j.neuropharm.2022.109204.

Insulin-like growth factor 1 regulates excitatory synaptic transmission in pyramidal neurons from adult prefrontal cortex

Shuwen Yue,

Yunwanbin Wang,

Zi-Jun Wang*

Department of Pharmacology & Toxicology, School of Pharmacy, University of Kansas, Lawrence, KS, USA

Abstract

Insulin-like growth factor 1 (IGF1) influences synaptic function in addition to its role in brain development and aging. Although the expression levels of IGF1 and IGF1 receptor (IGF1R) peak during development and decline with age, the adult brain has abundant IGF1 or IGF1R expression. Studies reveal that IGF1 regulates the synaptic transmission in neurons from young animals. However, the action of IGF1 on neurons in the adult brain is still unclear. Here, we used prefrontal cortical (PFC) slices from adult mice (~8 weeks old) to characterize the role of IGF1 on excitatory synaptic transmission in pyramidal neurons and the underlying molecular mechanisms. We first validated IGF1R expression in pyramidal neurons using translating ribosomal affinity purification assay. Then, using whole-cell patch-clamp recording, we found that IGF1 attenuated the amplitude of evoked excitatory postsynaptic current (EPSC) without affecting the frequency and amplitude of miniature EPSC. Furthermore, this decrease in excitatory neurotransmission was blocked by pharmacological inhibition of IGF1R or conditional knockdown of IGF1R in PFC pyramidal neurons. In addition, we determined that IGF1-induced decrease of EPSC amplitude was due to postsynaptic effect (internalization of a-amino-3-hydroxy-5-methyl-4-isoxazolepropionic acid receptors [AMPAR]) rather than presynaptic glutamate release. Finally, we found that inhibition of metabotropic glutamate receptor subtype-1 (mGluR1) abolished IGF1-induced attenuation of evoked EPSC amplitude and decrease of AMPAR expression at synaptic membrane, suggesting mGluR1-mediated endocytosis of AMPAR was involved. Taken together, these data provide the first evidence that IGF1 regulates excitatory synaptic transmission in adult PFC via the interaction between IGF1R-dependent signaling pathway and mGluR1-mediated AMPAR endocytosis.

*Corresponding author. Department of Pharmacology and Toxicology, School of Pharmacy, University of Kansas, 1251 Wescoe Hall Drive, Lawrence, KS 66045, USA. zjwang@ku.edu (Z.-J. Wang).

CRediT authorship contribution statement

Shuwen Yue: performed experiments, analyzed data, wrote part of the manuscript. **Yunwanbin Wang:** performed experiments, analyzed data. **Zi-Jun Wang:** designed experiments, supervised the project, and wrote the manuscript.

Declaration of competing interest

The authors report no competing financial or other interests.

Appendix A. Supplementary data

Supplementary data to this article can be found online at https://doi.org/10.1016/j.neuropharm.2022.109204.

Keywords

Insulin-like growth factor 1; Pyramidal neurons; Prefrontal cortex; Excitatory synaptic transmission; Evoked EPSC; IGF1R; Erk; mGluR1; AMPAR

1. Introduction

Insulin-like growth factor 1 (IGF1) is a neurotrophic factor involved in many cellular processes in the central nervous system (CNS), including the generation, differentiation and maturation of neurons (Brooker et al., 2000; Mir et al., 2017; Yuan et al., 2015). IGF1 has high affinity to IGF1 receptors (IGF1R), which are abundantly expressed in the CNS (Aguado et al., 1994; Araujo et al., 1989; Ayer-le Lievre et al., 1991; Bach et al., 1991; Bondy and Lee, 1993; Han et al., 1988; Sandberg et al., 1988). Besides its endocrinological and neurotrophic effects, IGF1/IGF1R system directly modulates neuronal firing and synaptic transmission (Cao et al., 2011; Fetterly et al., 2021; Gazit et al., 2016; Kakizawa et al., 2003; Pristera et al., 2019). For example, IGF1/IGF1R differentially regulates spontaneous and evoked excitatory synaptic transmission in CA1 pyramidal neurons (Gazit et al., 2016); IGF1 modulates midbrain dopaminergic neuronal firing (Pristera et al., 2019); IGF1R inhibition alters excitatory neurotransmission in medium spiny neurons (Fetterly et al., 2021). These studies indicate that IGF1/IGF1R system may have distinct impact on synaptic plasticity in different brain regions. However, the action of IGF1 on synaptic function in other brain regions is poorly understood, such as the prefrontal cortex (PFC).

PFC is a key brain region that controls higher-order functions (e.g., decision-making, working memory, attention, perception and emotion (Giustino and Maren, 2015; Koechlin et al., 2003; Liu et al., 2014a; Zhang et al., 2014)) and continues to develop during adolescence (Caballero et al., 2016; Larsen and Luna, 2018). Studies have shown that IGF1 regulates pyramidal neuron excitability in the infralimbic cortex (ventromedial part of PFC) from juvenile rodents (Maglio et al., 2021). However, very little is known about how IGF1/IGF1R system affects pyramidal neuron function in mature PFC. Furthermore, layer V excitatory neurons (pyramidal neurons) mainly send projections to other subcortical regions (e.g., striatum and ventral tegmental area) to coordinate information processing for behavioral control (Beckstead, 1979; Carr and Sesack, 2000; Gao et al., 2022; Gerfen et al., 2018; Vertes, 2004). Functional changes in these neurons have been implicated in many brain disorders, such as autism spectrum disorder (Stoner et al., 2014), depression (Pizzagalli and Roberts, 2022), substance use disorder (Goldstein and Volkow, 2011) and Alzheimer's diseases (Salat et al., 2001). Interestingly, altered IGF1/IGF1R signaling has been linked to these brain disorders (Garcia-Marchena et al., 2017; Gasparini and Xu, 2003; Kopczak et al., 2015; Pedraz et al., 2015; Reece, 2013), and IGF1 treatment can recover synaptic deficits related to several brain diseases (Castro et al., 2014; Linker et al., 2020). Therefore, it is critical to understand how IGF1 regulates synaptic transmission in pyramidal neurons in adult PFC.

Here, we investigated how IGF1 bath application affects excitatory synaptic transmission to layer V pyramidal neurons in PFC slices from adult mice (~8 weeks old). We

found that IGF1 attenuated evoked excitatory synaptic transmission mediated by α-amino-3-hydroxy-5-methyl-4-isoxazolepropionic acid receptor (AMPAR). This reduction of neurotransmission was blocked by IGF1R inhibitor, and was absent in mice with IGF1R conditional knockdown (cKD) in PFC pyramidal neurons. In addition, we demonstrated that IGF1R downstream kinases Erk1/2 were upregulated after IGF1 treatment, which was accompanied by increased surface expression of metabotropic glutamate receptor subunit-1 (mGluR1) and increased endocytosis of AMPAR. Furthermore, blocking mGluR1 abolished IGF1-mediated inhibition of excitatory neurotransmission and internalization of AMPAR. Therefore, our results demonstrate a key role of IGF1 in regulating excitatory synaptic transmission in layer V pyramidal neurons from adult PFC.

2. Material and methods

2.1. Animals

C57BL/6 mice, *Igf1r*$^{flox/flox}$ (*Igf1r*$^{f/f}$) mice (B6; 129-*Igf1r*^{tm2Arge}/J, 012251) and EGFP-L10a$^{flox/flox}$ (EGFP-L10a$^{f/f}$) mice (B6; 129S4-Gt (ROSA)26Sor$^{tm9(EGFP/Rpl10a)Amc}$/J, 024750) were obtained from Jackson Laboratory (Bar Harbor, ME, USA) and maintained in our lab. Genotyping for these mice were shown in sFig. 1. Current study used both male and female mice. Four to five mice were housed in one cage. Animals were housed under the temperature and humidity controlled by animal care facility with 12h light/dark cycle (lights on at 11:00 a.m. and lights off at 11:00 p.m.) with standard mouse chow and water *ad libitum*. All the procedures were approved by the Institutional Animal Care and Use Committee, University of Kansas. All animals were maintained according to the National Institutes of Health guidelines in Association for Assessment and Accreditation of Laboratory Animal Care accredited facilities.

2.2. Intracranial viral injection

Mice were deeply anesthetized with 100 mg/kg ketamine as well as 5 mg/kg xylazine and placed on a stereotaxic apparatus (RWD instruments, CA, USA). Body temperature was maintained with a heating pad throughout the surgery. pENN-AAV-CamKII-Cre-SV40-AAV9 (titer: 2×10^{13} GC/ml) or control virus CaMKIIa-P2A-mCherry-WPRE-AAV9 (titer: 2×10^{13} GC/ml) were purchased from Addgene (Watertown, MA, USA) and Biohippo (Rockville, MD, USA), respectively. Virus (300 nl/side) was delivered bilaterally into the dorsomedial PFC (AP: 2.0, ML: 0.3, DV:2.0). The injection was controlled by a minipump (KD Scientific, MA, USA) at the rate of 50 nl/min. The injection needle (10 μl, Hamilton, NV, USA) was kept in place for another 10 min for full dispersion of the virus. Electrophysiological and biochemical experiments were performed after 14 days of viral expression.

2.3. Translating ribosomal affinity purification (TRAP)

Ribosomal affinity purification was performed as previously described (Heiman et al., 2014; Martin et al., 2018) with modifications. In brief, EGFP-L10a$^{f/f}$ mice were deeply anesthetized with ketamine/xylazine and decapitated. Brains were quickly removed and placed on a pre-chilled coronal brain matrix. Brain slices (1 mm) were placed in ice-cold 0.01M PBS (phosphate-buffered saline) and tissue punches (2.0 mm diameter) containing

PFC were immediately homogenized in ice-cold supplemented homogenization buffer (50 mM Tris [pH 7.4], 100 mM KCl, 12 mM $MgCl_2$, 1% NP-40 plus RNase, 1 mM DTT, 100 μg/ml Cyclohexamide, 1 mg/ml Heparin, RNAsin (200 Units/ml) and protein inhibitors) in a glass homogenizer. Homogenates were centrifuged at 10,000 RPM for 10 min at 4 °C to pellet nuclei and large cell debris. 10% of the supernatant was taken out as input sample, and the rest was added to anti-GFP antibodies-coupled beads (HtzGFP-19F7 and HtzGFP-19C8, Memorial Sloan Kettering Cancer Center, NY, USA; Dyna magnetic beads coupled with recombinant protein G, 10003D, ThermoFisher Scientific, NH, USA) and rotated overnight at 4 °C. Polysome-RNA complexes bound to magnetic beads were washed three times for 5 min with high salt buffer (50 mM Tris [pH 7.4], 300 mM KCl, 12 mM $MgCl_2$, 1% NP-40, 1 mM dithiothreitol and 100 μg/ml cyclohexaminde), and then separated from the supernatant by a magnet rack. Then input and TRAP RNA were eluted and purified using the Absolutely RNA Nanoprep kit (400753, Agilent, CA, USA). RNA quantity and quality were determined by Nano Drop (ND-100; Thermo Fisher Scientific).

2.4. Quantitative real-time PCR

Input and TRAP RNA were purified as described above. Total mRNA was isolated from PFC punches using Trizol reagent (Invitrogen, CA, USA) and treated with Dnase I (Invitrogen) to remove genomic DNA. First strand complementary DNA (cDNA) was synthesized using PrimeScript™ Reverse Transcriptase (2680B, TaKaRa, CA, USA). Then the cDNA was amplified in the StepOnePlus™ Real-Time PCR System (Applied Biosystems, MA, USA) using PowerUp™ SYBR™ Green Master Mix (A25742, Applied Biosystems) and sequence-specific primers. *Gapdh* was used as a housekeeping gene for quantitation. Fold change was determined by: Fold change = $2^{-\Delta(\Delta C_T)}$, where $\Delta C_T = C_{T(gene\ of\ interest)} - C_{T(Gapdh)}$, and $\Delta(\Delta C_T) = \Delta C_{T(\text{treated group})} - \Delta C_{T(\text{control})}$. Primer sequences used were provided in Supplemental Table 1.

2.5. Electrophysiology

Whole-cell patch-clamp recording of pyramidal neurons in the PFC were performed as previously described (Wang et al., 2020, 2021, 2022). Brain tissue were rapidly removed and placed in ice-cold sucrose solution containing 220 mM sucrose, 15 mM HEPES, 11 mM glucose, 1 mM Na_2HPO_4, 4 mM $MgSO_4$, 0.1 mM $CaCl_2$, 2.5 mM KCl (pH 7.35, 300 mOsm). Coronal slices (300 μm) were cut using a vibratome (VT1000s, Leica, Wetzlar, Germany) and kept in transfer solution containing 132 mM NaIse, 15 mM HEPES, 23 mM glucose, 2 mM KCl, 4 mM $MgCl_2$, 0.1 mM $CaCl_2$ (pH 7.35, 300 mOsm). The slices were allowed to recover in oxygenated (95% O_2 and 5% CO_2) artificial cerebrospinal fluid (ACSF) (130 mM NaCl, 26 mM $NaHCO_3$, 3 mM KCl, 5 mM $MgCl_2$, 1.25 mM NaH_2PO_4, 1 mM $CaCl_2$, 10 mM glucose, pH 7.60, 300 mOsm) for 40 min in 33 °C water bath and then 30 min under room temperature.

Brain slice containing PFC was chosen according to mouse brain stereotaxic coordinates (Franklin and Paxinos, 2007): AP 2.0 from Bregma. Pyramidal neurons were visualized using a 40 × water-immersed lens with an upright microscope (Scientifica, East Sussex, UK). Then real-time image was acquired by video-enhanced infrared monochrome camera through IR-Capture software (Dage-MTI, IN, USA). Using the Measurement function, the

dorsomedial PFC brain region were identified according to the following parameters: 1.3–1.8 mm below the dorsal edge of the brain slice. Additionally, layer V pyramidal neurons within this area were targeted based on the perpendicular distance from midline: 0.3–0.5 mm (Mitric et al., 2019), as well as the pyramidal-shaped soma and long apical dendrites (Hearing et al., 2013). Finally, layer V pyramidal neurons in mice dorsomedial PFC were further identified by the following electrophysiology parameters: resting membrane potential < −55 mV, capacitance >100 pF with no spontaneous activity (Anderson et al., 2021; Connors and Gutnick, 1990; Hearing et al., 2013). To differentiate pyramidal neurons and interneurons, we recorded action potential evoked by different current steps and the synaptic-driven spontaneous action potential (a small depolarizing current [< 50 pA] was applied). Characterization of PFC layer V pyramidal neurons were provided in sFig. 2.

Patch pipette (3–6 MΩ) was pulled from 1.5 mm borosilicate glass capillaries using a micropipette puller (P-1000, Sutter Instrument, CA, USA) and filled with internal solution containing 130 mM Cs-methanesulfonate, 10 mM CsCl, 4 mM NaCl, 10 mM HEPES, 1 mM $MgCl_2$, 5 mM EGTA, 2 mM QX-314, 12 mM phosphocreatine, 5 mM MgATP, 0.2 mM Na_2GTP (pH 7.2–7.3, 265–270 mOsm). In some experiments, 2 μM jasplakinolide was added in internal solution and 15–20 min elapse after break-in was applied before recording. During recording the brain slices were perfused with oxygenated ACSF (1 ml/min) and bicuculline (20 μM) was added to isolate the excitatory transmission. For action potential recording in pyramidal neurons and interneurons, pipette was filled with 6 mM KCl, 124 mM K–gluconate, 10 mM HEPES, 1 mM $MgCl_2$, 5 mM EGTA, 0.5 mM $CaCl_2$, 3 mM Na_2ATP, 0.5 mM Na_2GTP, and 12 mM phosphocreatine.

Miniature EPSCs (mEPSCs) were recorded by holding neurons at −70 mV with the present of 1 μM tetrodotoxin (TTX). Evoked EPSCs (eEPSC) were elicited by a local stimulation generated by a stimulation isolator controlled by a pulse generator (A-M system, WA, USA). Stimulation pulses (0.06 ms, 70 μA) were delivered at 0.05 Hz to minimize short-term synaptic plasticity, and five traces of EPSCs were averaged. To ensure the stimulus was similar across different slices, the tip of the bipolar electrode (FHC, ME, USA) was carefully adjusted to ~20 μm below the surface of each slice (Liu et al., 2017) and 100 μm horizontally from recorded cell (Wang et al., 2020, 2021). To minimize experimental variations, layer V PFC pyramidal neurons with comparable membrane capacitances were included and patched cells whose series resistance changed by more than 10% were rejected (Wang et al., 2020, 2021; Zheng et al., 2019).

Data were acquired using an Multiclamp 700B amplifier (Molecular Devices, CA, USA), and digitized with a DigiData 1550B data acquisition board (Molecular Device). Cells were allowed to stabilize for at least 2 min before recording. The recorded signals were digitized at 5 kHz, filtered at 1 kHz, and collected using Clampex 11.0 data acquisition system (Molecular Devices). Baseline responses were established (10 min) followed by a bath application of IGF1 (0 nM, 1 nM and 10 nM, 15 min) and washout (30 or 45 min) in the presence or absence of IGF1R antagonists picropodophyllin (PPP, 500 nM, Selleck Chemicals, TX, USA) or mGluR1 antagonist LY367385 (100 μM, Sigma-Aldrich, MO, USA). The presynaptic glutamate release was measured using paired-pulse ratio (PPR). eEPSCs were measured across a range of interpulse intervals (20, 50, 100, 200 and 400

ms). The PPR was calculated by dividing the averaged amplitude of the second peak by the averaged amplitude of the first peak. Recorded mEPSC data were analyzed with miniAnalysis (Synaptosoft, NJ, USA). Cumulative distribution graphs were generated by sampling 50 random mEPSC events from each neuron in each condition that equally weighted each cell in that condition. Recorded eEPSC data were analyzed with Clamfit 11.0 software (Molecular Device).

Full-field glutamate uncaging experiment was carried out in the dark according to previous publications (Passlick and Ellis-Davies, 2018). MNI-caged-L-glutamate (MNI-Glu) was purchased from Tocris (1 mM, NE, USA) and dissolved in bath solution (ACSF supplemented with bicuculline and TTX). The concern about MNI-Glu-mediated inhibition of GABA-A receptor (Palma-Cerda et al., 2012) was cleared by the presence of bicuculline during recording. MNI-Glu was locally delivered through a glass pipette (diameter 5–6 μm) that was placed near patched cells (~30 μm, Fig. 4H, sFig. 6A) and controlled by continuous air pressure (~3 psi) generated with Picospritzer (Parker Instrumentation, Cleveland, OH, USA). Alexa fluor 555 was added to visualize the delivery of MNI-Glu through the pipette (sFig. 6B). Glutamate was uncaged by photolysis via UV light (360 nm) that was delivered by LED light source (CoolLED, UK) coupled through a 40× objective (Olympus, 0.8 numerical aperture). Light power was measured with a photometer (5 mW, Thorlabs, Newton, NJ, USA). UV Light (1–5 ms) was controlled and triggered by voltage modulation through DigiData 1550B (Molecular Device). DNQX (20 μM, Sigma) was applied to validate the AMPAR-mediated currents (sFig. 6C). Input-output curve was recorded to validate the synaptic response to glutamate uncaging (sFig. 6D).

2.6. Synaptosome fractionation and western blot

Membrane-associated proteins in synapses were prepared as described previously (Qin et al., 2018; Zhang et al., 2021). In brief, 8 PFC punches (diameter: 2 mm, thickness: 300 μm) from vehicle- or IGF1-incubated (10 nM, 15 min) mouse brain slices (300 μm) were collected and homogenized with 100 μl lysis buffer (15 mM Tris, pH 7.6, 0.25 M sucrose, 2 mM EDTA, 1 mM EGTA, 10 mM Na_3VO_4, 25 mM NaF, 10 mM $Na_4P_2O_7$, 1 mM PMSF and protease inhibitor cocktail). 20 μl homogenate was taken for total protein western blotting. The rest of the homogenate was centrifuged at 800×*g* for 5 min to remove nuclei and large debris, the remaining supernatant was then centrifuged at 10,000×*g* for 10 min to separate the cytosolic fractions (S) and synaptic fractions. The crude synaptosome fractions in the pellet were suspended in 100 μl Triton buffer (lysis buffer containing 1% Triton X-100 and 300 mM NaCl) and then centrifuged at 16,000×*g* for 15 min to separate the cytosolic proteins in synapses (P1, supernatant) and membrane-associated proteins in synapses (P2, pellet). The Triton insoluble pellet containing P2 fraction were further dissolved in 1% SDS. The protein samples were ready for western blotting.

Total protein samples and synaptic membrane-associated protein samples were heated with 4 × loading buffer at 90 °C for 5 min, separated by 7.5% SDS-PAGE and transferred onto NC membranes. Membranes were rinsed with TBST 5 min for 3 times, blocked with 5% nonfat dry milk in TBST for 1 h under room temperature, and then incubated at 4 °C overnight with primary antibodies against GluR1 (1:1000, 13185S, Cell Signaling

Technology, MA, USA), GluR2 (1:1000, 13607S, Cell Signaling Technology), IGF1R (1:1000, 3027, Cell Signaling Technology), p-IGF1R (1:1000, 3024s, Cell Signaling Technology), PSD95 (1:1000, 3450S, Cell Signaling Technology), p-synapsin I (1:1000, NB300-745, Novus Biologicals, CO, USA), synaptophysin (1:2500, 36406, Cell Signaling Technology), mGluR1 (1:500, ab82211, Abcam, MA, USA), Erk1/2 (1:1000, 4695S, Cell Signaling Technology), p-Erk1/2 (1:1000, 4370S, Cell Signaling Technology), tubulin (1:2000, T 9026-100UL, MillipreSigma, MA, USA) and β-actin (1:2000, 3700S, Cell Signaling Technology). Membranes were then washed, incubated with HRP-conjugated secondary antibody (1:2000, Mouse IgG HRP Linked Whole Ab: GENA931-1 ML, Rabbit IgG HRP Linked Whole Ab: GENA934-1 ML, Sigma-Aldrich) for 1 h under room temperature. After another three washes, membranes were imaged with chemiluminescence detecting substrate (ThermoFisher Scientific). Images were acquired using a Gel DOX imaging system (Bio-Rad Laboratories, CA, USA) then analyzed using Image J. Full blots for representative blots are provided in sFig. 10.

2.7. Immunohistochemistry

Immunohistochemistry and analysis were performed as previously descried with modifications (Singh et al., 2022). Mice were deeply anesthetized with ketamine/xylazine and transcardially perfused with sterile-filtered 0.01 M PBS, pH 7.4 followed by sterile-filtered 4% paraformaldehyde (PFA) in 0.01 M PBS, pH 7.4 at 4 °C. Whole brains were immediately harvested and post-fixed in 4% PFA at 4 °C for 24 h and then immersed in 30% sucrose in 0.01 M PBS (pH 7.4) at 4 °C for cryoprotection. Coronal sections encompassing the PFC were cut at a thickness of 40 μm using a vibratome (Leica VT1000s) then stored at −20 °C until use. For immunostaining, brain sections were rinsed in 0.01 M PBS (pH 7.4) for 3 times then blocked with 3% normal donkey serum (NDS, Jackson ImmunoResearch, PA, USA) in PBS containing 0.3% Triton-X for 1 h at room temperature. Sections were then incubated with primary antibody IGF1R (1:500, Abcam, ab190289) diluted in 3% NDS in PBS with 0.1% saponin overnight at 4 °C. On the second day, after 3 PBS washes, sections were incubated with anti-rabbit Alexa Fluor 488-conjugated secondary antibody at 1:500 (ThermoFisher Scientific) for 2 h at room temperature. Coverslips were attached to the slides with mounting media (Vector lab, CA, USA). Images were acquired using a Leica Laser Scanning Confocal Upright Microscope or an Olympus Inverted Epifluorescence Microscope. All specimens were imaged under identical conditions and analyzed with identical parameters using Image J.

2.8. Statistical analysis

All statistical analyses were performed with GraphPad Prism and SPSS. Experiments with more than two dependent variables were subjected to multi-factor ANOVA followed with Bonferroni correction for multiple post hoc comparisons. Experiments with two groups were analyzed statistically using two-tailed unpaired t-tests. All data were presented as the mean ± SEM. Sample sizes were determined based on power analyses and were similar to those reported in previous works (Wang et al., 2015, 2020, 2021, 2022). Statistical details are provided in Supplementary Table 2.

3. Results

3.1. The expression level of IGF1R in pyramidal neurons from adult PFC

To determine the expression level of IGF1R in pyramidal neurons from adult PFC, we employed TRAP method to isolate pyramidal neuron-enriched mRNA using adult GFP-L10a$^{f/f}$ mice (Fig. slA). In GFP-L10a$^{f/f}$ mice, the expression of GFP-L10a fusion gene is blocked by a loxP-flanked STOP fragment (Liu et al., 2014b) (Fig. 1A). Cre-recombinase will result in the expression of GFP-tagged L10a in Cre-expressing cells (Fig. 1A-B). After injecting CaMKII-Cre-mCherry-AAV into the PFC of GFP-L10a$^{f/f}$ mice, we first validated that GFP-expressing cells overlapped with mCherry^{+} cells (Fig. 1C), suggesting GFP expression was only turned on with Cre presence. Furthermore, we performed TRAP assay to pull down GFP-L10a-associated mRNAs using anti-GFP antibody (Heiman et al., 2014) (Fig. 1B). Compared to total mRNAs (inputs, Fig. 1D), CaMKII-Cre-mediated TRAP (CaMKII-TRAP) mRNAs showed significant enrichment of marker genes for excitatory pyramidal neurons including PSD95 (*Dlg4,* $t_{(8)} = 4.73$, $p = 0.0015$; N = 4–6/group), SH3 and multiple ankyrin repeat domains protein 1 (*Shank1*, $t_{(5)} = 3.42$, $p = 0.0188$; N = 3–4/group), and N-methyl D-aspartate receptor subtype 2B (*Grin2b,* $t_{(4)} = 3.08$, $p = 0.0369$; N = 3/group). In addition, CaMKII-TRAP mRNAs also showed obvious depletion of marker genes for oligodendrocytes (myelin oligodendrocyte glycoprotein [*Mog]* $t_{(5)} = 4.96$, $p = 0.0042$, N = 3–4/group; transcription factor SOX-10 [*Sox10*] $t_{(8)} = 2.86$, $p = 0.0211$, N = 4–6/group), microglia (e.g., cluster of differentiation molecule 11B [*CD11b*], $t_{(5)} = 10.99$, $p = 0.0001$, N = 3–4/group; C-X3-C motif chemokine receptor 1 [*Cx3cr1*], $t_{(8)} = 7.39$, $p < 0.001$, N = 4–6/group), and astrocytes (e.g., aldehyde dehydrogenase 1 family member L1 [*Aldh1l1*], $t_{(8)} = 3.84$, $p = 0.0049$, N = 4–6/group). Additionally, we found that *Igf1r* gene expression level in pyramidal neuron-enriched mRNA was comparable to the expression level in total mRNA (Fig. 1E; N = 5/group). Moreover, immunostaining studies (Fig. 1F-G) revealed that CaMKII-mCherry-AAV-infected neurons (red) showed obvious IGF1R protein expression (green). Additionally, IGF1R protein expression was presented at layers II-VI (Fig. 1G). These data suggest that adult PFC pyramidal neurons have abundant IGF1R expression.

3.2. IGF1 differentially regulates mEPSC and eEPSC in pyramidal neurons from adult PFC

Next, we sought to determine the effect of IGF1 on excitatory synaptic transmission in pyramidal neurons from adult PFC. As dorsomedial and ventromedial part of PFC have different projections (Vertes, 2004), and the role of IGF1 on neurotransmission in adult dorsomedial PFC is completely unknown, we restricted our electrophysiology studies in dorsomedial PFC. PFC slices from adult wild type (WT) mouse were prepared and perfused with different concentrations of IGF1 (0, 1 and 10 nM) for 15 min followed by 45-min washout. We found that IGF1 did not affect the frequency and amplitude of mEPSCs at any given dose (Fig. 2A-B, sFig. 3A-B, N = 7 cells from 3 mice for 0 nM, N = 7 cells from 3 mice for 1 nM and N = 7 cells from 4 mice for 10 nM). Consistently, we found no change in the cumulative distribution of both inter-event interval and amplitude of mEPSC (Fig. 2C-E').

As mEPSC and stimulation-evoked EPSC are mediated through different mechanisms (Horvath et al., 2020; Kavalali, 2015; Peled et al., 2014; Sara et al., 2011; Sudhof, 2013), we then examined how IGF1 affects eEPSC in pyramidal neurons. We found that IGF1 significantly decreased the amplitude of eEPSC at a saturation dose 10 nM (Ster et al., 2005; Tu et al., 2021), whereas 0 and 1 nM IGF1 did not induce any changes in eEPSC amplitude (Fig. 3A, sFig. 4A, $F_{(2, 18)} = 4.28$, p = 0.0302; multi-factor rmANOVA, N = 5 cells from 3 mice for 0 nM, N = 5 cells from 3 mice for 1 nM and N = 11 cells from 5 mice for 10 nM). Furthermore, the eEPSC amplitude returned to baseline level after 30-min washout. Because IGF1 mainly signals through IGF1R (with low affinity for insulin receptor)(Fernandez and Torres-Aleman, 2012; O'Kusky et al., 2000), we next determined whether IGF1-mediated decrease of eEPSC amplitude was dependent on IGF1R. To this end, we applied a selective IGF1R antagonist PPP at an effective dose 500 nM (Labouebe et al., 2013). We performed control experiments to examine the effect of PPP inhibition on eEPSC amplitude. Fifteen-min of PPP bath application slightly increased eEPSC amplitude but did not reach statistical significance (sFig. 4B). Furthermore, our data showed that when PPP was applied before 10 nM IGF1, the decrease of eEPSC amplitude was absent (Fig. 3B, sFig. 4C, N = 7 cells from 4 mice). In addition, neither PPP pretreatment before IGF1 application (sFig. 4D-G) nor PPP inhibition alone (sFig. 4H-I) altered the frequency and amplitude of mEPSC.

As PPP bath application prevented IGF1R action in all cell types, we next used Cre-LoxP system to conditionally knock down IGF1R expression in adult PFC pyramidal neurons to examine if IGF1 action is dependent on IGF1R expression in pyramidal neurons. *Igf1r*$^{f/f}$ mice (Dietrich et al., 2000) possess loxP sites on either side of exon 3 of *Igf1r* gene (Fig. 3C). Cre-recombinase can result in exon 3 deletion in Cre-expressing cells. We injected CaMKII-Cre-mCherry-AAV into the PFC of adult *Igf1r*$^{f/f}$ mice to induce IGF1R cKD in pyramidal neurons. We found that CaMKII-Cre-mCherry-AAV resulted in a significant decrease of IGF1R protein expression in pyramidal neurons (Fig. 3D-E, IGF1R: $t_{(19)} = 4.04$, $p = 0.0007$, N = 9–12 slices from 3 to 4 mice/group) as compared to control virus (CaMKII-mCherry-AAV). Western blot studies using bulk PFC tissue also showed a significant reduction of IGF1R protein level after IGF1R cKD in PFC pyramidal neurons (Fig. 3F-G, $t_{(13)} = 4.94$, $p = 0.0003$, N = 7–8/group). Furthermore, using primers against either *Igf1r* gene exon 3 (P1) or exon 13 and exon 14 junction (P2, Fig. 3C), we found that *Igf1r* mRNA level was also significantly lower in the PFC from mice received CaMKII-Cre-mCherry-AAV injection (Fig. 3H; P1: $t_{14} = 3.00$, $p = 0.0096$; P2: $t_{14} = 2.46$, $p = 0.0275$; N = 8/group) as compared to controls (mice received CaMKII-mCherry-AAV). Of note, we did not find complete knockdown of *Igf1r* exon3 in bulk PFC tissue, which was likely due to IGF1R cKD being restricted to pyramidal neurons. Using this validated Cre-LoxP system, we found that IGF1R cKD in PFC pyramidal neurons blocked IGF1-induced decrease of eEPSC amplitudes (Fig. 3I-J, sFig. 4J, N = 7 cells from 3 mice). We next used a higher dose of IGF1 (30 nM) to test whether the lack of IGF1 action in IGF1R cKD neurons are due to insufficient agonist-receptor interaction. We found that there was no change in EPSC amplitude after IGF1 30 nM treatment (Fig. 3I, sFig. 4J). Together these data suggest that IGF1-mediated inhibition of eEPSC amplitude in adult PFC pyramidal neurons were dependent on IGF1R in these neurons.

3.3. IGF1 treatment decreased AMPAR expression level at synaptic membrane

As IGF1-mediated inhibition of excitatory synaptic transmission could be mediated by decrease in presynaptic glutamate release or postsynaptic glutamate transmission, we first measured PPR to determine the presynaptic effect. No change in PPR was found after 15-min 10 nM IGF1 bath application (Fig. 4A; N = 5 cells from 3 mice). Synapsins are a family of neuron-specific phosphoproteins that regulate neurotransmitter release (e.g., glutamate release (Chi et al., 2001; Hilfiker et al., 1999; Nichols et al., 1992)) via facilitating the synaptic vesicle movement to the membrane for fusion. Therefore, we next tested whether IGF1 batch application could affect synapsin I activity in synaptic cytosol to further validate the effect of IGF1 on presynaptic release. We validated our synaptosome fractionation method by probing the proteins that are enriched in different fractions. Our data showed that PSD95 was enriched in membrane-associated synaptic proteins (P2 fraction) and that synaptophysin was enriched in cytosolic proteins in synapses (P1 fraction, sFig. 5), which are in agreement with previous publications (Gardoni et al., 2006; Henson et al., 2012; Qin et al., 2018; Zhang et al., 2021). We showed that there was no change in the protein level of *p*-synapsin I (Fig. 4B-C; N = 4/group) at synaptic-cytosolic fraction (P1) after 10 nM IGF1 treatment, which is consistent with unaltered PPR. Taken together, these data suggest that the presynaptic mechanism is not involved in the effect of IGF1 on excitatory transmission in pyramidal neurons in adult PFC.

Then we further investigated the postsynaptic mechanism by determining the expression level of AMPAR at synaptic membrane. We found that 10 nM IGF1 bath application induced significant decreases of glutamate receptor AMPA type subunit 1 (GluR1, $t_{(12)} = 2.70$, $p = 0.0194$, N = 6–8/group) and subunit 2 (GluR2, $t_{(13)} = 2.60$, $p = 0.0219$, N = 7–8/group) expression levels at synaptic membrane (P2 fraction, Fig. 4D-E), without affecting GluR1 and GluR2 levels in total protein lysate (Fig. 4F-G; N = 6/group). To further validate the postsynaptic effect, we performed glutamate uncaging experiment (Fig. 4H, sFig. 6). MNI-Glu (1 mM) was locally applied to patched pyramidal neurons and released by UV light (360 nm, sFig. 6A-B). TTX and bicuculline were added in ACSF to block action potential-evoked presynaptic neurotransmitters release and inhibitory postsynaptic currents, respectively. We found that photo uncaged glutamate induced reliable excitatory postsynaptic currents, which can be blocked by AMPAR blocker DNQX (20 μM, sFig. 6C-D). Interestingly, we found that IGF1 significantly reduced glutamate-evoked EPSC amplitude (Fig. 4I, sFig. 6E, $F_{(1, 9)} = 25.44$, p = 0.0007; multi-factor rmANOVA, N = 5 cells from 3 mice for 0 nM, and N = 6 cells from 3 mice for 10 nM), which was reminiscent of electrode-stimulated EPSCs (Fig. 3A). These data indicate that IGF1-induced decrease of excitatory transmission in pyramidal neurons in adult PFC is associated with decreased AMPAR expression levels at postsynaptic membrane.

Although AMPAR endocytosis has clathrin- and dynamin-dependent or independent mechanisms (Carroll et al., 1999; Lin et al., 2000; Man et al., 2000), both constitutive and regulative AMPA receptor endocytosis rely on actin dynamics (Glebov et al., 2015; Xiao et al., 2001; Zhou et al., 2001). The actin depolymerization at the initial phase can facilitate the dissociation of AMPARs from their anchor on the postsynaptic membrane, which allows the released AMPARs to diffuse for further endocytosis (Zhou et al., 2001). We further used

pharmacological tools to test whether blocking AMPAR endocytosis by stabilizing actin filaments can affect IGF1-mediated EPSC depression. Two μM Jasplakinolide (Jas, a drug that stabilize actin filaments) was added into internal solution as previously reported (Xiao et al., 2001). We found that including Jas in the recording pipette blocked IGF1-induced inhibition of eEPSCs (sFig. 7). These data further suggested that AMPAR internalization is involved in the IGF1 action.

3.4. IGF1 treatment triggered mGluR1-mediated AMPAR endocytosis

Next, we examined the potential molecular mechanisms underlying IGF1 action on AMPAR occupancy at postsynaptic membrane. Our previous data showed that IGF1 action was dependent on IGF1R expression in pyramidal neurons (Fig. 3). Upon IGF1R activation, tyrosine kinase activity in its β-subunits was activated for autophosphorylation to trigger downstream signaling cascades, such as mitogen activated protein (MAP) kinase pathway involving in regulation of synaptic plasticity (Sweatt, 2001; Thomas and Huganir, 2004). Therefore, we determined the protein expression level of MAPK pathway components. We found that 15-min 10 nM IGF1 bath application significantly increased the protein levels of p-IGF1R ($t_{(10)} = 4.33$, $p = 0.0015$, N = 6/group) and p-Erk 1/2 ($t_{(10)} = 2.37$, $p = 0.0395$, N = 6/group), whereas the level of total IGF1R and Erk1/2 (N = 6/group) remained unaffected (Fig. 5A-B).

Studies have shown that Erk1/2 can directly phosphorylate mGluR1 (Yang et al., 2017) and that activation of mGluR1 can lead to the rapid internalization of AMPAR from synaptic membrane (Snyder et al., 2001). Therefore, we next investigated the expression level of mGluR1 on synaptic membrane. We found that 15-min 10 nM IGF1 application significantly increased the protein level of mGluR1 at synaptic membrane (P2 fraction, $t_{(10)} = 2.89$, $p = 0.016$, N = 6/group), without affecting mGluR1 level in total protein extracts (N = 4/group, Fig. 6A-B). We hypothesized that more mGluR1 inserted into synaptic membrane can facilitate the endocytosis of AMPAR and blocking mGluR1 may prevent the reduction of AMPAR function. To test this, we applied selective mGluR1 antagonist LY367385 (100 μM (Ennis et al., 2006)) before IGF1 bath application. We first performed control experiment to determine whether mGluR1 inhibition affects baseline eESPC amplitudes. We found that LY367385 application itself did not change eEPSC amplitude (sFig. 8A-B). Furthermore, mGluR1 antagonist LY367385 pretreatment completely abolished the inhibition effect of IGF1 on eEPSC amplitude (Fig. 6C, sFig. 8C, N = 5 cells from 3 mice), as well as IGF1-induced reduction of GluR1 and GluR2 expression levels at synaptic membrane (Fig. 6D-E; N = 6/group). Taken together, our data showed that the inhibition effect of IGF1 on eEPSC amplitude was mediated through mGluR1-induced AMPAR endocytosis.

4. Discussion

4.1. IGF1/IGF1R system regulates synaptic transmission in an age-, cell type- and brain region-specific manner

The expression levels of IGF1 and IGF1R fluctuate throughout lifetime: the expression levels of IGF1 and IGF1R peak during developmental stage, but both IGF1 and IGF1R are widely presented in adult human and rodent brain (Aguado et al., 1994; Araujo et al.,

1989; Ayer-le Lievre et al., 1991; Bach et al., 1991; Bondy and Lee, 1993; Han et al., 1988; Sandberg et al., 1988). IGF1 in the brain can be locally produced by all cell types (with a diffuse expression pattern in the cortex) (Bach et al., 1991), and circulating IGF1 can also enter the brain through choroid plexus and blood brain barrier (Carro et al., 2000, 2002; Nishijima et al., 2010; Trejo et al., 2001). Compared to the low expression of IGF1 mRNA in adult brain, IGF1R was abundantly expressed in many brain regions including the PFC (Baron-Van Evercooren et al., 1991; Bondy, 1991). Our data further showed that there is abundant IGF1R expression in CaMKII-expressing neurons (pyramidal neurons) from adult PFC (Fig. 1), which may potentially contribute to the effect of IGF1 on synaptic plasticity. One limitation for our experiment is that TRAP method does not reveal information about layer-specific expression of *Igf1r* gene. Although we tried to target layer V of PFC, the CaMKII-AAV virus can still diffuse to other regions. Our immunohistostaining data proved that IGF1R protein expression is abundant in layer II-VI pyramidal neurons (Fig. 1F-G), but future studies using techniques with layer specific resolution are needed to reveal the expression pattern of *Igf1r* gene in pyramidal neurons from different layers.

Studies using cultured neurons or young rodents reported that IGF1/IGF1R system regulates neurotransmitter release and synaptic transmission through pre- and/or post-synaptic mechanisms (Araujo et al., 1989; Castro-Alamancos and Torres-Aleman, 1993; Gazit et al., 2016; Nilsson et al., 1988; Nunez et al., 2003; Seto et al., 2002; Wang and Linden, 2000). For example, in cultured hippocampal pyramidal neurons or 2-month-old hippocampal slices (CA1 region), IGF1R tone enhances or diminishes evoked or spontaneous excitatory synaptic transmission via modulating presynaptic mitochondria-dependent Ca^{2+} transient and ATP production (Gazit et al., 2016). In layer II/III pyramidal neurons from barrel cortex, IGF1 induces long-term depression (LTD) of inhibitory synaptic transmission by stimulating astrocyte Ca_{2+} signaling and the A2a adenosine receptors at presynaptic inhibitory terminals (Noriega-Prieto et al., 2021). In dorsal column nuclei cells from brain stem, IGF1 treatment increases the amplitude of evoked excitatory postsynaptic potential through a presynaptic facilitation (Nunez et al., 2003). In Purkinje neurons from mouse embryonic cerebellar culture, IGF1 induces LTD of excitatory synaptic transmission that requires postsynaptic Clathrin-mediated GluR2 endocytosis (Wang and Linden, 2000). In ventromedial PFC layer V pyramidal neurons from young mice (P20-30), IGF1 inhibits excitatory synaptic transmission through a presynaptic dependent mechanism (Maglio et al., 2021). Here, our study indicates that in adult dorsomedial PFC layer V pyramidal neurons, IGF1 regulates excitatory synaptic transmission through a postsynaptic effect that is dependent on mGluR1-mediated GluR1 and GluR2 endocytosis (Fig. 4). All these studies highlight that the action of IGF1 on synaptic transmission is highly dependent on the developmental stages, cell types and brain regions.

Of note, IGF1 is also involved in the regulation of inhibitory synaptic transmission. For example, exogenous IGF1 could rescue synaptotagmin-10 knockout-induced reduction of inhibitory postsynaptic currents (IPSC) in cultured olfactory bulb neurons (Cao et al., 2011); vasoactive intestinal peptide (VIP)-expressing neuron-derived IGF1 increases inhibitory synaptic input onto VIP neurons (Mardinly et al., 2016) in visual cortex from young mice (P19–P21); and IGF1 reduces IPSC in ventromedial PFC layer V pyramidal neurons from young mice (P20-30) (Maglio et al., 2021). While others showed that IGF1 exposure only

affects excitatory but not inhibitory postsynaptic markers (Corvin et al., 2012). In addition, IGF1 analog (des-IGF1 (Clemmons et al., 1992)) does not alter N-methyl-D-aspartate (NMDAR)-mediated EPSC in CA1 pyramidal neurons from young rats (P20-40) (Ramsey et al., 2005). Under our recording condition, IPSC was completely blocked by the presence of bicuculline; and by holding cells at −70 mV, the voltage-dependent magnesium (Mg^{2+}) block of NMDA currents (Johnson and Ascher, 1990) was present. Therefore, future studies will be needed to dissect out how IGF1 affects IPSC and NMDAR-mediated synaptic currents in pyramidal neurons from adult PFC.

4.2. IGF1/IGF1R signaling pathway interacts with AMPAR trafficking

The diminished synaptic transmission induced by IGF1 bath application depends on IGF1R-mediated signaling pathway. IGF1 mainly signals through IGF1R, which recruits downstream kinases cascades (e.g., PI3K-Akt and MAPK pathways) (Fernandez and Torres-Aleman, 2012; O'Kusky et al., 2000) to modulate gene transcription and other signaling branches (Davila et al., 2007; Dyer et al., 2016). IGF1 also has low affinity for insulin receptors (IR). Recent studies have shown that mTORC1 and PI3K/Akt singling are favorably regulated by IR, while a cluster of proteins preferentially phosphorylated after IGF1R activation are enriched in Erk2-phosphorylated sites (Nagao et al., 2021). Our data showed that phosphorylated Erk1/2 is increased after IGF1 bath application, suggesting activation of MAPK cascade plavs an important role in the action of IGF1.

MAPK cascade is essential for synaptic plasticity (Sweatt, 2001; Thomas and Huganir, 2004). For example, Erk signaling is involved in long-term potentiation (LTP) via facilitating CaMKII-mediated phosphorylation of GluR1 and its synaptic trafficking (English and Sweatt, 1997; Zhu et al., 2002). In addition, MAPK signaling pathway activation is also essential for the induction of LTD (Kawasaki et al., 1999). Studies have shown that Erk1/2 directly bind to and phosphorylate mGluR1 to maintain its synaptic insertion (Yang et al., 2017), which can facilitate AMPAR endocytosis to mediate LTD (Snyder et al., 2001). We found that IGF1 bath application can increase the expression level of mGluR1 at the synaptic membrane, which may facilitate AMPAR endocytosis. This hypothesis is supported by our data showing IGF1-induced reduction of GluR1 and GluR2 levels at synaptic membrane (Fig. 4), which were blocked by mGluR1 inhibitor pre-treatment (Fig. 6). Of note, we found that the IGF1-weakened AMPAR synaptic transmission lasted for about 30 min, which was shorter than typical LTD (>50 min). This may suggest that other counteracting mechanisms recovering AMPAR-mediated neurotransmission may be also activated after IGF1 treatment, such as PI3K-Akt signaling pathway interplaying with mTORC1 cascades to facilitate AMPAR translation (Duman et al., 2016); or IGF1 indirectly activating PKA (Cheng et al., 2014) to phosphorylate GluR1 at Ser845 (Roche et al., 1996) to enhance AMPAR currents.

It is noteworthy that studies have shown that neurotrophins activating Erk1/2 can stimulate synapsin I phosphorylation to affect glutamate release (Jovanovic et al., 2000). Erk1/2 stoichiometrically phosphorylates synapsin I at Ser-62 and Ser-67 (residues 58–72 of synapsin I, also referred as P-site 4/5) (Jovanovic et al., 1996; Matsubara et al., 1996). We found that IGF1 bath application did not alter phosphorylated synapsin I at Ser-62 and

Ser-67 sites, which is consistent with lack of presynaptic effects in EPSC recording (Fig. 4). These results further suggest that IGF1-induced reduction of eEPSC amplitude is attributed to postsynaptic effect.

4.3. mGluR1-mediated AMPAR trafficking may depend on neurotransmitter release

Our studies indicate that the amplitudes of miniature EPSC and evoked EPSC are differentially regulated by IGF1 bath application. Spontaneous and stimulation-evoked neurotransmission differ in the neurotransmitter release pattern and postsynaptic targets (Horvath et al., 2020; Kavalali, 2015; Peled et al., 2014; Sara et al., 2011; Sudhof, 2013). For example, spontaneous release typically results from fusion of a single synaptic vesicle that contains about 8000 glutamate molecules (Wang et al., 2019) and only elicits a small postsynaptic response (Fatt and Katz, 1952; Postlethwaite et al., 2007; Wang et al., 2019). Glutamate receptors are generally far from saturation during quantal transmission (Liu et al., 1999; Mainen et al., 1999). Therefore, even after IGF1-triggered AMPAR endocytosis (mediated by mGluR1), there still are sufficient AMPARs at postsynaptic membrane to mediate spontaneous synaptic events (sFig. 9).

On the contrary, low frequency stimulation induces synchronous release, which is the release of readily releasable pool of vesicles (Alabi and Tsien, 2012) that usually consists of 1–2 dozens of quanta per synapse (Rosenmund and Stevens, 1996; Stevens and Tsujimoto, 1995) and generates large postsynaptic currents. Stimulation-induced action potential-driven neurotransmission results in significant glutamate release, which can occupy a large number of postsynaptic AMPAR to induce large postsynaptic current. Therefore, IGF1-triggered AMPAR endocytosis will significantly affect the amplitude of evoked EPSC (sFig. 9). Additionally, stimulation-evoked neurotransmission is supported by more synapses with high release probability (P(r)); whereas spontaneous neurotransmission is supported by more low-P(r) synapses (Peled et al., 2014). Moreover, mGluR1-mediated AMPAR trafficking can be influenced by the probability of glutamate release: mGluR1-dependent synaptic weakening does not occur at synapses with low P(r) (Sanderson et al., 2018). Therefore, IGF1R may be enriched at synapses with high P(r) in adult PFC to mediate IGF1 action preferentially on evoked neurotransmission (i.e., attenuation of eEPSC amplitude). Additionally, our extracellular electrical stimulation (bulk stimulation) evokes action potentials in axons from multiple neurons to release vesicles from multiple terminals (Lines et al., 2017; Nowak and Bullier, 1998; Rattay, 1999), which lacks the single-synapse resolution to determine whether IGF1/IGF1R system has similar or distinct effect on unitary EPSCs from different types of monosynaptic connections onto layer V pyramidal neurons. Therefore, future studies are needed to further understand how IGF1/IGF1R system regulate excitatory synaptic transmission in adult PFC at single-synapse level.

4.4. The potential role of the crosstalk between neuron and astrocyte

The tripartite synapses play key roles in regulation of neuronal activity and synaptic transmission (Araque et al., 1999). Studies have shown that gliotransmitters can suppress or enhance synaptic transmission. For example, astrocytes-released glutamate increases excitatory postsynaptic currents through extra-synaptic NMDAR (Araque et al., 1998) or presynaptic group I mGluR (Fiacco and McCarthy, 2004). Astrocytes-released adenosine

triphosphate or adenosine can activate P2 receptor or adenosine A1 or 2A receptor to suppress excitatory synaptic transmission (Panatier et al., 2011; Zhang et al., 2003). These mechanisms rely on activity dependent presynaptic neurotransmitter release and play critical roles in mediating synaptic depression (Durkee et al., 2021).

Additionally, astrocytes also have abundant IGF1R expression. Astrocytic activation of IGF1R influences Ca^{2+} function (Noriega-Prieto et al., 2021), which is critical for action potential-driven gliotransmitter release. Therefore, based on current results, we cannot fully exclude the possibility that the differential regulation of eEPSC and mEPSC by IGF1 may also attribute to the gliotransmitters release from astrocytes. Studies have shown that neuronal IGF1R activation increases probability of neuronal firing (Gazit et al., 2016; Maglio et al., 2021; Pristera et al., 2019), which can consequently increase the release of synaptic glutamate. Synaptic glutamate together with astrocytic IGF1R activation can activate astrocytes to facilitate the release of gliotransmitter to suppress synaptic transmission and induce synaptic depression (Fig. 3A). On the contrary, when action potential is absent (blocked by TTX), there will be no presynaptic release of glutamate to activate astrocytes. Therefore, mEPSC is not suppressed by IGF1 application (Fig. 2). Although we found that IGF1 suppressed glutamate-evoked EPSC with the presence of TTX (Fig. 4I), which suggests limited presynaptic effect, the potential role of postsynaptic effect that may involve astrocytes still needs further elucidation.

5. Conclusion

Taken together, our data indicate that IGF1 bath application reduces evoked excitatory synaptic transmission mediated by AMPAR without affecting spontaneous neurotransmission in layer V pyramidal neurons from adult PFC. This effect is dependent on IGF1R expression at PFC pyramidal neurons. Meanwhile, IGF1-inudced reduction of eEPSC amplitude is associated with decreased surface expression of GluR1 and GluR2, which is potentially mediated by mGluR1, as blocking mGluR1 prevents IGF1-induced decrease of synaptic transmission and reduction of GluR1 and GluR2 levels at synaptic membrane. IGF1 treatment increases phosphorylation of IGF1R and downstream kinases Erk1/2, which may stabilize mGluR1 at synaptic membrane to facilitate AMPAR endocytosis. These results provide electrophysiological and molecular mechanisms for IGF1-dependent synaptic plasticity in pyramidal neurons from adult PFC. As altered IGF1/IGF1R system has been implicated in many brain disorders with disrupted PFC function (e.g., Alzheimer’s disease (Gasparini and Xu, 2003), depression (Kopczak et al., 2015) and substance use disorders (Garcia-Marchena et al., 2017; Pedraz et al., 2015; Reece, 2013)), our results will also shed light on future studies to investigate whether and how neuronal and/or astrocytic IGF1/IGF1R system in the PFC is involved in the neurobiology of these brain disorders.

Supplementary Material

Refer to Web version on PubMed Central for supplementary material.

Acknowledgements

We thank Dr. Archana Singh, Kegan Hertel and Anasuya Subramanian for their technical support. We thank University of Kansas Microscopy and Analytical Imaging core for the technical support. This study was supported by NIH grant DA050908 (Z.-J. W.), University of Kansas start-up funding, and University of Kansas General Research Fund allocation 2302023 (NFRD Fund to Z.-J. W.).

References

Aguado F, Sanchez-Franco F, Rodrigo J, Cacicedo L, Martinez-Murillo R, 1994. Insulin-like growth factor I-immunoreactive peptide in adult human cerebellar Purkinje cells: co-localization with low-affinity nerve growth factor receptor. Neuroscience 59, 641–650. [PubMed: 8008211]

Alabi AA, Tsien RW, 2012. Synaptic vesicle pools and dynamics. Cold Spring Harbor Perspect. Biol 4, a013680.

Anderson EM, Engelhardt A, Demis S, Porath E, Hearing MC, 2021. Remifentanil self-administration in mice promotes sex-specific prefrontal cortex dysfunction underlying deficits in cognitive flexibility. Neuropsychopharmacology 46, 1734–1745. [PubMed: 34012018]

Araque A, Parpura V, Sanzgiri RP, Haydon PG, 1999. Tripartite synapses: glia, the unacknowledged partner. Trends Neurosci. 22, 208–215. [PubMed: 10322493]

Araque A, Sanzgiri RP, Parpura V, Haydon PG, 1998. Calcium elevation in astrocytes causes an NMDA receptor-dependent increase in the frequency of miniature synaptic currents in cultured hippocampal neurons. J. Neurosci 18, 6822–6829. [PubMed: 9712653]

Araujo DM, Lapchak PA, Collier B, Chabot JG, Quirion R, 1989. Insulin-like growth factor-1 (somatomedin-C) receptors in the rat brain: distribution and interaction with the hippocampal cholinergic system. Brain Res. 484, 130–138. [PubMed: 2540883]

Ayer-le Lievre C, Stahlbom PA, Sara VR, 1991. Expression of IGF-I and -II mRNA in the brain and craniofacial region of the rat fetus. Development 111, 105–115. [PubMed: 2015788]

Bach MA, Shen-Orr Z, Lowe WL Jr., Roberts CT Jr., LeRoith D, 1991. Insulin-like growth factor I mRNA levels are developmentally regulated in specific regions of the rat brain. Brain Res. Mol. Brain Res 10, 43–48. [PubMed: 1647481]

Baron-Van Evercooren A, Olichon-Berthe C, Kowalski A, Visciano G, Van Obberghen E, 1991. Expression of IGF-I and insulin receptor genes in the rat central nervous system: a developmental, regional, and cellular analysis. J. Neurosci. Res 28, 244–253. [PubMed: 1851850]

Beckstead RM, 1979. An autoradiographic examination of corticocortical and subcortical projections of the mediodorsal-projection (prefrontal) cortex in the rat. J. Comp. Neurol 184, 43–62. [PubMed: 762282]

Bondy CA, 1991. Transient IGF-I gene expression during the maturation of functionally related central projection neurons. J. Neurosci 11, 3442–3455. [PubMed: 1658250]

Bondy CA, Lee WH, 1993. Patterns of insulin-like growth factor and IGF receptor gene expression in the brain. Functional implications. Ann. N. Y. Acad. Sci 692, 33–43. [PubMed: 8215043]

Brooker GJ, Kalloniatis M, Russo VC, Murphy M, Werther GA, Bartlett PF, 2000. Endogenous IGF-1 regulates the neuronal differentiation of adult stem cells. J. Neurosci. Res 59, 332–341. [PubMed: 10679768]

Caballero A, Granberg R, Tseng KY, 2016. Mechanisms contributing to prefrontal cortex maturation during adolescence. Neurosci. Biobehav. Rev 70, 4–12. [PubMed: 27235076]

Cao P, Maximov A, Sudhof TC, 2011. Activity-dependent IGF-1 exocytosis is controlled by the Ca(2+)-sensor synaptotagmin-10. Cell 145, 300–311. [PubMed: 21496647]

Carr DB, Sesack SR, 2000. Projections from the rat prefrontal cortex to the ventral tegmental area: target specificity in the synaptic associations with mesoaccumbens and mesocortical neurons. J. Neurosci 20, 3864–3873. [PubMed: 10804226]

Carro E, Nunez A, Busiguina S, Torres-Aleman I, 2000. Circulating insulin-like growth factor I mediates effects of exercise on the brain. J. Neurosci 20, 2926–2933. [PubMed: 10751445]

Carro E, Trejo JL, Gomez-Isla T, LeRoith D, Torres-Aleman I, 2002. Serum insulin-like growth factor I regulates brain amyloid-beta levels. Nat. Med 8, 1390–1397. [PubMed: 12415260]

Carroll RC, Beattie EC, Xia H, Luscher C, Altschuler Y, Nicoll RA, Malenka RC, von Zastrow M, 1999. Dynamin-dependent endocytosis of ionotropic glutamate receptors. Proc. Natl. Acad. Sci. U. S. A 96, 14112–14117. [PubMed: 10570207]

Castro-Alamancos MA, Torres-Aleman I, 1993. Long-term depression of glutamate-induced gamma-aminobutyric acid release in cerebellum by insulin-like growth factor I. Proc. Natl. Acad. Sci. U. S. A 90, 7386–7390. [PubMed: 8346260]

Castro J, Garcia RI, Kwok S, Banerjee A, Petravicz J, Woodson J, Mellios N, Tropea D, Sur M, 2014. Functional recovery with recombinant human IGF1 treatment in a mouse model of Rett Syndrome. Proc. Natl. Acad. Sci. U. S. A 111, 9941–9946. [PubMed: 24958891]

Cheng CW, Adams GB, Perin L, Wei M, Zhou X, Lam BS, Da Sacco S, Mirisola M, Quinn DI, Dorff TB, Kopchick JJ, Longo VD, 2014. Prolonged fasting reduces IGF-1/PKA to promote hematopoietic-stem-cell-based regeneration and reverse immunosuppression. Cell Stem Cell 14, 810–823. [PubMed: 24905167]

Chi P, Greengard P, Ryan TA, 2001. Synapsin dispersion and reclustering during synaptic activity. Nat. Neurosci 4, 1187–1193. [PubMed: 11685225]

Clemmons DR, Dehoff ML, Busby WH, Bayne ML, Cascieri MA, 1992. Competition for binding to insulin-like growth factor (IGF) binding protein-2, 3, 4, and 5 by the IGFs and IGF analogs. Endocrinology 131, 890–895. [PubMed: 1379166]

Connors BW, Gutnick MJ, 1990. Intrinsic firing patterns of diverse neocortical neurons. Trends Neurosci. 13, 99–104. [PubMed: 1691879]

Corvin AP, Molinos I, Little G, Donohoe G, Gill M, Morris DW, Tropea D, 2012. Insulin-like growth factor 1 (IGF1) and its active peptide (1-3)IGF1 enhance the expression of synaptic markers in neuronal circuits through different cellular mechanisms. Neurosci. Lett 520, 51–56. [PubMed: 22609570]

Davila D, Piriz J, Trejo JL, Nunez A, Torres-Aleman I, 2007. Insulin and insulin-like growth factor I signalling in neurons. Front. Biosci 12, 3194–3202. [PubMed: 17485293]

Dietrich P, Dragatsis I, Xuan S, Zeitlin S, Efstratiadis A, 2000. Conditional mutagenesis in mice with heat shock promoter-driven ere transgenes. Mamm. Genome 11, 196–205. [PubMed: 10723724]

Duman RS, Aghajanian GK, Sanacora G, Krystal JH, 2016. Synaptic plasticity and depression: new insights from stress and rapid-acting antidepressants. Nat. Med. 22, 238–249. [PubMed: 26937618]

Durkee C, Kofuji P, Navarrete M, Araque A, 2021. Astrocyte and neuron cooperation in long-term depression. Trends Neurosci. 44, 837–848. [PubMed: 34334233]

Dyer AH, Vahdatpour C, Sanfeliu A, Tropea D, 2016. The role of Insulin-Like Growth Factor 1 (IGF-1) in brain development, maturation and neuroplasticity. Neuroscience 325, 89–99. [PubMed: 27038749]

English JD, Sweatt JD, 1997. A requirement for the mitogen-activated protein kinase cascade in hippocampal long term potentiation. J. Biol. Chem 272, 19103–19106. [PubMed: 9235897]

Ennis M, Zhu M, Heinbockel T, Hayar A, 2006. Olfactory nerve-evoked, metabotropic glutamate receptor-mediated synaptic responses in rat olfactory bulb mitral cells. J. Neurophysiol 95, 2233–2241. [PubMed: 16394070]

Fatt P, Katz B, 1952. Spontaneous subthreshold activity at motor nerve endings. J. Physiol 117, 109–128. [PubMed: 14946732]

Fernandez AM, Torres-Aleman I, 2012. The many faces of insulin-like peptide signalling in the brain. Nat. Rev. Neurosci 13, 225–239. [PubMed: 22430016]

Fetterly TL, Oginsky MF, Nieto AM, Alonso-Caraballo Y, Santana-Rodriguez Z, Ferrario CR, 2021. Insulin bidirectionally alters NAc glutamatergic transmission: interactions between insulin receptor activation, endogenous opioids, and glutamate release. J. Neurosci 41, 2360–2372. [PubMed: 33514676]

Fiacco TA, McCarthy KD, 2004. Intracellular astrocyte calcium waves in situ increase the frequency of spontaneous AMPA receptor currents in CA1 pyramidal neurons. J. Neurosci 24, 722–732. [PubMed: 14736858]

Franklin KBJ, Paxinos G, 2007. The Mouse Brain in Stereotaxic Coordinates, third ed. Academic Press.

Gao L, Liu S, Gou L, Hu Y, Liu Y, Deng L, Ma D, Wang H, Yang Q, Chen Z, Liu D, Qiu S, Wang X, Wang D, Wang X, Ren B, Liu Q, Chen T, Shi X, Yao H, Xu C, Li CT, Sun Y, Li A, Luo Q, Gong H, Xu N, Yan J, 2022. Single-neuron projectome of mouse prefrontal cortex. Nat. Neurosci 25, 515–529. [PubMed: 35361973]

Garcia-Marchena N, Silva-Pena D, Martin-Velasco AI, Villanua MA, Araos P, Pedraz M, Maza-Quiroga R, Romero-Sanchiz P, Rubio G, Castilla-Ortega E, Suarez J, Rodriguez de Fonseca F, Serrano A, Pavon FJ, 2017. Decreased plasma concentrations of BDNF and IGF-1 in abstinent patients with alcohol use disorders. PLoS One 12, e0187634. [PubMed: 29108028]

Gardoni F, Picconi B, Ghiglieri V, Polli F, Bagetta V, Bernardi G, Cattabeni F, Di Luca M, Calabresi P, 2006. A critical interaction between NR2B and MAGUK in L-DOPA induced dyskinesia. J. Neurosci 26, 2914–2922. [PubMed: 16540568]

Gasparini L, Xu H, 2003. Potential roles of insulin and IGF-1 in Alzheimer's disease. Trends Neurosci. 26, 404–406. [PubMed: 12900169]

Gazit N, Vertkin I, Shapira I, Helm M, Slomowitz E, Sheiba M, Mor Y, Rizzoli S, Slutsky I, 2016. IGF-1 receptor differentially regulates spontaneous and evoked transmission via mitochondria at hippocampal synapses. Neuron 89, 583–597. [PubMed: 26804996]

Gerfen CR, Economo MN, Chandrashekar J, 2018. Long distance projections of cortical pyramidal neurons. J. Neurosci. Res 96, 1467–1475. [PubMed: 27862192]

Giustino TF, Maren S, 2015. The role of the medial prefrontal cortex in the conditioning and extinction of fear. Front. Behav. Neurosci 9, 298. [PubMed: 26617500]

Glebov OO, Tigaret CM, Mellor JR, Henley JM, 2015. Clathrin-independent trafficking of AMPA receptors. J. Neurosci 35, 4830–4836. [PubMed: 25810514]

Goldstein RZ, Volkow ND, 2011. Dysfunction of the prefrontal cortex in addiction: neuroimaging findings and clinical implications. Nat. Rev. Neurosci 12, 652–669. [PubMed: 22011681]

Han VK, Lund PK, Lee DC, D'Ercole AJ, 1988. Expression of somatomedin/insulin-like growth factor messenger ribonucleic acids in the human fetus: identification, characterization, and tissue distribution. J. Clin. Endocrinol. Metab 66, 422–429. [PubMed: 2448331]

Hearing M, Kotecki L, Marron Fernandez de Velasco E, Fajardo-Serrano A, Chung HJ, Lujan R, Wickman K, 2013. Repeated cocaine weakens GABA(B)-Girk signaling in layer 5/6 pyramidal neurons in the prelimbic cortex. Neuron 80, 159–170. [PubMed: 24094109]

Heiman M, Kulicke R, Fenster RJ, Greengard P, Heintz N, 2014. Cell type-specific mRNA purification by translating ribosome affinity purification (TRAP). Nat. Protoc 9, 1282–1291. [PubMed: 24810037]

Henson MA, Larsen RS, Lawson SN, Perez-Otano I, Nakanishi N, Lipton SA, Philpot BD, 2012. Genetic deletion of NR3A accelerates glutamatergic synapse maturation. PLoS One 7, e42327. [PubMed: 22870318]

Hilfiker S, Pieribone VA, Czernik AJ, Kao HT, Augustine GJ, Greengard P, 1999. Synapsins as regulators of neurotransmitter release. Philos. Trans. R. Soc. Lond. B Biol. Sci 354, 269–279. [PubMed: 10212475]

Horvath PM, Piazza MK, Monteggia LM, Kavalali ET, 2020. Spontaneous and evoked neurotransmission are partially segregated at inhibitory synapses. Elife 9.

Johnson JW, Ascher P, 1990. Voltage-dependent block by intracellular Mg2+ of N-methyl-D-aspartate-activated channels. Biophys. J 57, 1085–1090. [PubMed: 1692749]

Jovanovic JN, Benfenati F, Siow YL, Sihra TS, Sanghera JS, Pelech SL, Greengard P, Czernik AJ, 1996. Neurotrophins stimulate phosphorylation of synapsin I by MAP kinase and regulate synapsin I-actin interactions. Proc. Natl. Acad. Sci. U. S. A 93, 3679–3683. [PubMed: 8622996]

Jovanovic JN, Czernik AJ, Fienberg AA, Greengard P, Sihra TS, 2000. Synapsins as mediators of BDNF-enhanced neurotransmitter release. Nat. Neurosci 3, 323–329. [PubMed: 10725920]

Kakizawa S, Yarnada K, Iino M, Watanabe M, Kano M, 2003. Effects of insulin-like growth factor I on climbing fibre synapse elimination during cerebellar development. Eur. J. Neurosci 17, 545–554. [PubMed: 12581172]

Kavalali ET, 2015. The mechanisms and functions of spontaneous neurotransmitter release. Nat. Rev. Neurosci 16, 5–16. [PubMed: 25524119]

Kawasaki H, Fujii H, Gotoh Y, Morooka T, Shimohama S, Nishida E, Hirano T, 1999. Requirement for mitogen-activated protein kinase in cerebellar long term depression. J. Biol. Chem 274, 13498–13502. [PubMed: 10224117]

Koechlin E, Ody C, Kouneiher F, 2003. The architecture of cognitive control in the human prefrontal cortex. Science 302, 1181–1185. [PubMed: 14615530]

Kopczak A, Stalla GK, Uhr M, Lucae S, Hennings J, Ising M, Holsboer F, Kloiber S, 2015. IGF-I in major depression and antidepressant treatment response. Eur. Neuropsychopharmacol 25, 864–872. [PubMed: 25836355]

Labouebe G, Liu S, Dias C, Zou H, Wong JC, Karunakaran S, Clee SM, Phillips AG, Boutrel B, Borgland SL, 2013. Insulin induces long-term depression of ventral tegmental area dopamine neurons via endocannabinoids. Nat. Neurosci 16, 300–308. [PubMed: 23354329]

Larsen B, Luna B, 2018. Adolescence as a neurobiological critical period for the development of higher-order cognition. Neurosci. Biobehav. Rev 94, 179–195. [PubMed: 30201220]

Lin JW, Ju W, Foster K, Lee SH, Ahmadian G, Wyszynski M, Wang YT, Sheng M, 2000. Distinct molecular mechanisms and divergent endocytotic pathways of AMPA receptor internalization. Nat. Neurosci 3, 1282–1290. [PubMed: 11100149]

Lines J, Covelo A, Gomez R, Liu L, Araque A, 2017. Synapse-specific regulation revealed at single synapses is concealed when recording multiple synapses. Front. Cell. Neurosci 11, 367. [PubMed: 29218000]

Linker SB, Mendes APD, Marchetto MC, 2020. IGF-1 treatment causes unique transcriptional response in neurons from individuals with idiopathic autism. Mol. Autism 11, 55. [PubMed: 32591005]

Liu D, Gu X, Zhu J, Zhang X, Han Z, Yan W, Cheng Q, Hao J, Fan H, Hou R, Chen Z, Chen Y, Li CT, 2014a. Medial prefrontal activity during delay period contributes to learning of a working memory task. Science 346, 458–463. [PubMed: 25342800]

Liu G, Choi S, Tsien RW, 1999. Variability of neurotransmitter concentration and nonsaturation of postsynaptic AMPA receptors at synapses in hippocampal cultures and slices. Neuron 22, 395–409. [PubMed: 10069344]

Liu J, Krautzberger AM, Sui SH, Hofmann OM, Chen Y, Baetscher M, Grgic I, Kumar S, Humphreys BD, Hide WA, McMahon AP, 2014b. Cell-specific translational profiling in acute kidney injury. J. Clin. Invest 124, 1242–1254. [PubMed: 24569379]

Liu Z, Chen Z, Shang C, Yan F, Shi Y, Zhang J, Qu B, Han H, Wang Y, Li D, Sudhof TC, Cao P, 2017. IGF1-Dependent synaptic plasticity of mitral cells in olfactory memory during social learning. Neuron 95, 106–122 e105. [PubMed: 28683263]

Maglio LE, Noriega-Prieto JA, Maroto IB, Martin-Cortecero J, Munoz-Callejas A, Callejo-Mostoles M, Fernandez de Sevilla D, 2021. IGF-1 facilitates extinction of conditioned fear. Elife 10.

Mainen ZF, Malinow R, Svoboda K, 1999. Synaptic calcium transients in single spines indicate that NMDA receptors are not saturated. Nature 399, 151–155. [PubMed: 10335844]

Man HY, Lin JW, Ju WH, Ahmadian G, Liu L, Becker LE, Sheng M, Wang YT, 2000. Regulation of AMPA receptor-mediated synaptic transmission by clathrin-dependent receptor internalization. Neuron 25, 649–662. [PubMed: 10774732]

Mardinly AR, Spiegel I, Patrizi A, Centofante E, Bazinet JE, Tzeng CP, Mandel-Brehm C, Harmin DA, Adesnik H, Fagiolini M, Greenberg ME, 2016. Sensory experience regulates cortical inhibition by inducing IGF1 in VIP neurons. Nature 531, 371–375. [PubMed: 26958833]

Martin JA, Caccamise A, Werner CT, Viswanathan R, Polanco JJ, Stewart AF, Thomas SA, Sim FJ, Dietz DM, 2018. A novel role for oligodendrocyte precursor cells (OPCs) and Sox10 in mediating cellular and behavioral responses to heroin. Neuropsychopharmacology 43, 1385–1394. [PubMed: 29260792]

Matsubara M, Kusubata M, Ishiguro K, Uchida T, Titani K, Taniguchi H, 1996. Site-specific phosphorylation of synapsin I by mitogen-activated protein kinase and Cdk5 and its effects on physiological functions. J. Biol. Chem 271, 21108–21113. [PubMed: 8702879]

Mir S, Cai W, Carlson SW, Saatman KE, Andres DA, 2017. IGF-1 mediated neurogenesis involves a novel RIT1/akt/Sox2 cascade. Sci. Rep 7, 3283. [PubMed: 28607354]

Mitric M, Seewald A, Moschetti G, Sacerdote P, Ferraguti F, Kummer KK, Kress M, 2019. Layer- and subregion-specific electrophysiological and morphological changes of the medial prefrontal cortex in a mouse model of neuropathic pain. Sci. Rep 9, 9479. [PubMed: 31263213]

Nagao H, Cai W, Wewer Albrechtsen NJ, Steger M, Batista TM, Pan H, Dreyfuss JM, Mann M, Kahn CR, 2021. Distinct signaling by insulin and IGF-1 receptors and their extra- and intracellular domains. Proc. Natl. Acad. Sci. U. S. A 118.

Nichols RA, Chilcote TJ, Czernik AJ, Greengard P, 1992. Synapsin I regulates glutamate release from rat brain synaptosomes. J. Neurochem 58, 783–785. [PubMed: 1345942]

Nilsson L, Sara VR, Nordberg A, 1988. Insulin-like growth factor 1 stimulates the release of acetylcholine from rat cortical slices. Neurosci. Lett 88, 221–226. [PubMed: 3380358]

Nishijima T, Piriz J, Duflot S, Fernandez AM, Gaitan G, Gomez-Pinedo U, Verdugo JM, Leroy F, Soya H, Nunez A, Torres-Aleman I, 2010. Neuronal activity drives localized blood-brain-barrier transport of serum insulin-like growth factor-I into the CNS. Neuron 67, 834–846. [PubMed: 20826314]

Noriega-Prieto JA, Maglio LE, Zegarra-Valdivia JA, Pignatelli J, Fernandez AM, Martinez-Rachadell L, Fernandes J, Nunez A, Araque A, Torres-Aleman I, Fernandez de Sevilla D, 2021. Astrocytic IGF-IRs induce adenosine-mediated inhibitory downregulation and improve Sensory discrimination. J. Neurosci 41, 4768–4781. [PubMed: 33911021]

Nowak LG, Bullier J, 1998. Axons, but not cell bodies, are activated by electrical stimulation in cortical gray matter. I. Evidence from chronaxie measurements. Exp. Brain Res 118, 477–488. [PubMed: 9504843]

Nunez A, Carro E, Torres-Aleman I, 2003. Insulin-like growth factor I modifies electrophysiological properties of rat brain stem neurons. J. Neurophysiol 89, 3008–3017. [PubMed: 12612011]

O'Kusky JR, Ye P, D'Ercole AJ, 2000. Insulin-like growth factor-I promotes neurogenesis and sy nap to genesis in the hippocampal dentate gyrus during postnatal development. J. Neurosci 20, 8435–8442. [PubMed: 11069951]

Palma-Cerda F, Auger C, Crawford DJ, Hodgson AC, Reynolds SJ, Cowell JK, Swift KA, Cais O, Vyklicky L, Corrie JE, Ogden D, 2012. New caged neurotransmitter analogs selective for glutamate receptor sub-types based on methoxynitroindoline and nitrophenylethoxycarbonyl caging groups. Neuropharmacology 63, 624–634. [PubMed: 22609535]

Panatier A, Vallee J, Haber M, Murai KK, Lacaille JC, Robitaille R, 2011. Astrocytes are endogenous regulators of basal transmission at central synapses. Cell 146, 785–798. [PubMed: 21855979]

Passlick S, Ellis-Davies GCR, 2018. Comparative one- and two-photon uncaging of MNI-glutamate and MNI-kainate on hippocampal CAI neurons. J. Neurosci. Methods 293, 321–328. [PubMed: 29051090]

Pedraz M, Martin-Velasco AI, Garcia-Marchena N, Araos P, Serrano A, Romero-Sanchiz P, Suarez J, Castilla-Ortega E, Barrios V, Campos-Cloute R, Ruiz JJ, Torrens M, Chowen JA, Argente J, de la Torre R, Santin LJ, Villanua MA, Rodriguez de Fonseca F, Pavon FJ, 2015. Plasma concentrations of BDNF and IGF-1 in abstinent cocaine users with high prevalence of substance use disorders: relationship to psychiatric comorbidity. PLoS One 10, e0118610. [PubMed: 25734326]

Peled ES, Newman ZL, Isacoff EY, 2014. Evoked and spontaneous transmission favored by distinct sets of synapses. Curr. Biol 24, 484–493. [PubMed: 24560571]

Pizzagalli DA, Roberts AC, 2022. Prefrontal cortex and depression. Neuropsychopharmacology 47, 225–246. [PubMed: 34341498]

Postlethwaite M, Hennig MH, Steinert JR, Graham BP, Forsythe ID, 2007. Acceleration of AMPA receptor kinetics underlies temperature-dependent changes in synaptic strength at the rat calyx of Held. J. Physiol 579, 69–84. [PubMed: 17138605]

Pristera A, Blomeley C, Lopes E, Threlfell S, Merlini E, Burdakov D, Cragg S, Guillemot F, Ang SL, 2019. Dopamine neuron-derived IGF-1 controls dopamine neuron firing, skill learning, and exploration. Proc. Natl. Acad. Sci. U. S. A 116, 3817–3826. [PubMed: 30808767]

Qin L, Ma K, Wang ZJ, Hu Z, Matas E, Wei J, Yan Z, 2018. Social deficits in Shank3-deficient mouse models of autism are rescued by histone deacetylase (HDAC) inhibition. Nat. Neurosci 21, 564–575. [PubMed: 29531362]

Ramsey MM, Adams MM, Ariwodola OJ, Sonntag WE, Weiner JL, 2005. Functional characterization of des-IGF-1 action at excitatory synapses in the CA1 region of rat hippocampus. J. Neurophysiol 94, 247–254. [PubMed: 15985695]

Rattay F, 1999. The basic mechanism for the electrical stimulation of the nervous system. Neuroscience 89, 335–346. [PubMed: 10077317]

Reece AS, 2013. Elevated IGF1 in clinical opiate dependence. Neuroendocrinol. Lett 34, 18–26. [PubMed: 23524620]

Roche KW, O'Brien RJ, Mammen AL, Bernhardt J, Huganir RL, 1996. Characterization of multiple phosphorylation sites on the AMPA receptor GluR1 subunit. Neuron 16, 1179–1188. [PubMed: 8663994]

Rosenmund C, Stevens CF, 1996. Definition of the readily releasable pool of vesicles at hippocampal synapses. Neuron 16, 1197–1207. [PubMed: 8663996]

Salat DH, Kaye JA, Janowsky JS, 2001. Selective preservation and degeneration within the prefrontal cortex in aging and Alzheimer disease. Arch. Neurol 58, 1403–1408. [PubMed: 11559311]

Sandberg AC, Engberg C, Lake M, von Holst H, Sara VR, 1988. The expression of insulin-like growth factor I and insulin-like growth factor II genes in the human fetal and adult brain and in glioma. Neurosci. Lett 93, 114–119. [PubMed: 3211366]

Sanderson TM, Bradley CA, Georgiou J, Hong YH, Ng AN, Lee Y, Kim HD, Kim D, Amici M, Son GH, Zhuo M, Kim K, Kaang BK, Kim SJ, Collingridge GL, 2018. The probability of neurotransmitter release governs AMPA receptor trafficking via activity-dependent regulation of mGluR1 surface expression. Cell Rep. 25, 3631–3646 e3633. [PubMed: 30590038]

Sara Y, Bal M, Adachi M, Monteggia LM, Kavalali ET, 2011. Use-dependent AMPA receptor block reveals segregation of spontaneous and evoked glutamatergic neurotransmission. J. Neurosci 31, 5378–5382. [PubMed: 21471372]

Seto D, Zheng WH, McNicoll A, Collier B, Quirion R, Kar S, 2002. Insulin-like growth factor-I inhibits endogenous acetylcholine release from the rat hippocampal formation: possible involvement of GABA in mediating the effects. Neuroscience 115, 603–612. [PubMed: 12421625]

Singh A, Xie Y, Davis A, Wang ZJ, 2022. Early social isolation stress increases addiction vulnerability to heroin and alters c-Fos expression in the mesocorticolimbic system. Psychopharmacology (Berl).

Snyder EM, Philpot BD, Huber KM, Dong X, Fallon JR, Bear MF, 2001. Internalization of ionotropic glutamate receptors in response to mGluR activation. Nat. Neurosci 4, 1079–1085. [PubMed: 11687813]

Ster J, Colomer C, Monzo C, Duvoid-Guillou A, Moos F, Alonso G, Hussy N, 2005. Insulin-like growth factor-1 inhibits adult supraoptic neurons via complementary modulation of mechanoreceptors and glycine receptors. J. Neurosci 25, 2267–2276. [PubMed: 15745952]

Stevens CF, Tsujimoto T, 1995. Estimates for the pool size of releasable quanta at a single central synapse and for the time required to refill the pool. Proc. Natl. Acad. Sci. U. S. A 92, 846–849. [PubMed: 7846064]

Stoner R, Chow ML, Boyle MP, Sunkin SM, Mouton PR, Roy S, Wynshaw-Boris A, Colamarino SA, Lein ES, Courchesne E, 2014. Patches of disorganization in the neocortex of children with autism. N. Engl. J. Med 370, 1209–1219. [PubMed: 24670167]

Sudhof TC, 2013. Neurotransmitter release: the last millisecond in the life of a synaptic vesicle. Neuron 80, 675–690. [PubMed: 24183019]

Sweatt JD, 2001. The neuronal MAP kinase cascade: a biochemical signal integration system subserving synaptic plasticity and memory. J. Neurochem 76, 1–10. [PubMed: 11145972]

Thomas GM, Huganir RL, 2004. MAPK cascade signalling and synaptic plasticity. Nat. Rev. Neurosci 5, 173–183. [PubMed: 14976517]

Trejo JL, Carro E, Torres-Aleman I, 2001. Circulating insulin-like growth factor I mediates exercise-induced increases in the number of new neurons in the adult hippocampus. J. Neurosci 21, 1628–1634. [PubMed: 11222653]

Tu X, Jain A, Decker H, Yasuda R, 2021. Local Autocrine Signaling of IGF1 Synthesized and Released by CA1 Pyramidal Neurons Regulates Plasticity of Dendritic Spines. Biorixv.

Vertes RP, 2004. Differential projections of the infralimbic and prelimbic cortex in the rat. Synapse 51, 32–58. [PubMed: 14579424]

Wang Y, Fathali H, Mishra D, Olsson T, Keighron JD, Skibicka KP, Cans AS, 2019. Counting the number of glutamate molecules in single synaptic vesicles. J. Am. Chem. Soc 141, 17507–17511. [PubMed: 31644274]

Wang YT, Linden DJ, 2000. Expression of cerebellar long-term depression requires postsynaptic clathrin-mediated endocytosis. Neuron 25, 635–647. [PubMed: 10774731]

Wang Z-J, Shwani T, Liu J, Zhong P, Yang F, Schatz K, Zhang F, Pralle A, Yan Z, 2022. Molecular and Cellular Mechanisms for Differential Effects of Chronic Social Isolation Stress in Males and Females. Molecular Psychiatry Epub ahead of print.

Wang ZJ, Rein B, Zhong P, Williams J, Cao Q, Yang F, Zhang F, Ma K, Yan Z, 2021. Autism risk gene KMT5B deficiency in prefrontal cortex induces synaptic dysfunction and social deficits via alterations of DNA repair and gene transcription. Neuropsychopharmacology 46, 1617–1626. [PubMed: 34007043]

Wang ZJ, Zhang XQ, Cui XY, Cui SY, Yu B, Sheng ZF, Li SJ, Cao Q, Huang YL, Xu YP, Zhang YH, 2015. Glucocorticoid receptors in the locus coeruleus mediate sleep disorders caused by repeated corticosterone treatment. Sci. Rep 5, 9442. [PubMed: 25801728]

Wang ZJ, Zhong P, Ma K, Seo JS, Yang F, Hu Z, Zhang F, Lin L, Wang J, Liu T, Matas E, Greengard P, Yan Z, 2020. Amelioration of autism-like social deficits by targeting histone methyltransferases EHMT1/2 in Shank3-deficient mice. Mol. Psychiatr 25, 2517–2533.

Xiao MY, Zhou Q, Nicoll RA, 2001. Metabotropic glutamate receptor activation causes a rapid redistribution of AMPA receptors. Neuropharmacology 41, 664–671. [PubMed: 11640920]

Yang JH, Mao LM, Choe ES, Wang JQ, 2017. Synaptic ERK2 phosphorylates and regulates metabotropic glutamate receptor 1 in vitro and in neurons. Mol. Neurobiol 54, 7156–7170. [PubMed: 27796752]

Yuan H, Chen R, Wu L, Chen Q, Hu A, Zhang T, Wang Z, Zhu X, 2015. The regulatory mechanism of neurogenesis by IGF-1 in adult mice. Mol. Neurobiol 51, 512–522. [PubMed: 24777577]

Zhang F, Rein B, Zhong P, Shwani T, Conrow-Graham M, Wang ZJ, Yan Z, 2021. Synergistic inhibition of histone modifiers produces therapeutic effects in adult Shank3-deficient mice. Transl. Psychiatry 11, 99. [PubMed: 33542189]

Zhang JM, Wang HK, Ye CQ, Ge W, Chen Y, Jiang ZL, Wu CP, Poo MM, Duan S, 2003. ATP released by astrocytes mediates glutamatergic activity-dependent heterosynaptic suppression. Neuron 40, 971–982. [PubMed: 14659095]

Zhang S, Xu M, Kamigaki T, Hoang Do JP, Chang WC, Jenvay S, Miyamichi K, Luo L, Dan Y, 2014. Selective attention. Long-range and local circuits for top-down modulation of visual cortex processing. Science 345, 660–665. [PubMed: 25104383]

Zheng Y, Liu A, Wang ZJ, Cao Q, Wang W, Lin L, Ma K, Zhang F, Wei J, Matas E, Cheng J, Chen GJ, Wang X, Yan Z, 2019. Inhibition of EHMT1/2 rescues synaptic and cognitive functions for Alzheimer's disease. Brain 142, 787–807. [PubMed: 30668640]

Zhou Q, Xiao M, Nicoll RA, 2001. Contribution of cytoskeleton to the internalization of AMPA receptors. Proc. Natl. Acad. Sci. U. S. A 98, 1261–1266. [PubMed: 11158627]

Zhu JJ, Qin Y, Zhao M, Van Aelst L, Malinow R, 2002. Ras and Rap control AMPA receptor trafficking during synaptic plasticity. Cell 110, 443–455. [PubMed: 12202034]

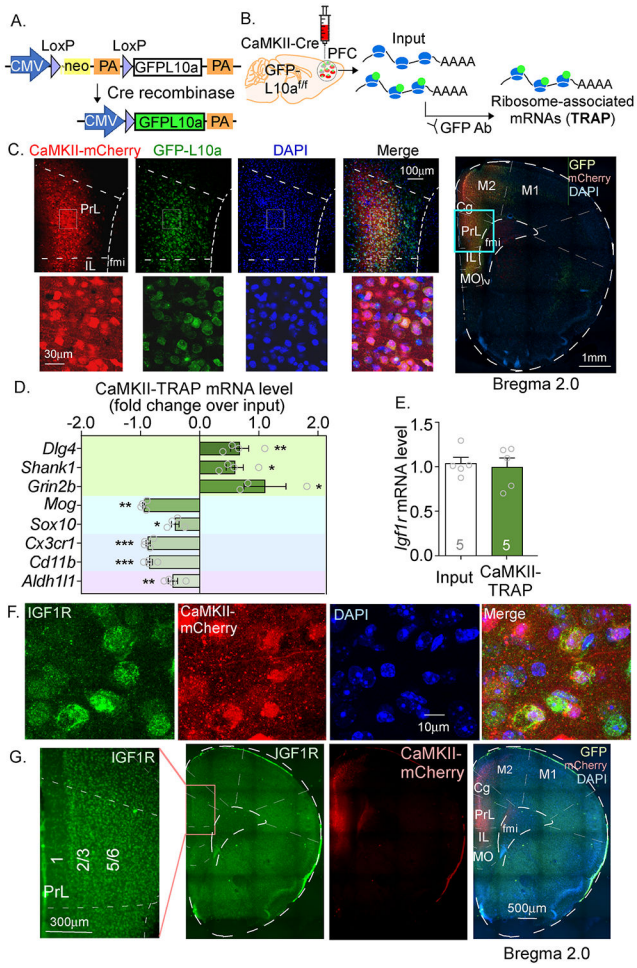

Fig. 1.

IGF1R expression in pyramidal neurons from adult PFC. A. Schematic of GFP-L10a allele and its recombined products with Cre presence. B. Schematic of translating ribosome affinity purification (TRAP) assay by GFP antibody pull down. C. Representative images of brain sections captured in PFC (prelimbic part, PrL; infralimbic part, IL) showing co-localization of CaMKII-Cre-mCheriy (red), GFP-L10a expression (green) and DAPI (blue) in adult GFP-L10a$^{f/f}$ mice. D. Bar graph showing the fold change (over input [total mRNA]) of mRNA level of marker genes for different cell types in CaMKII-Cre virus mediated TRAP (CaMKII-TRAP) mRNA from PFC of GFP-L10a$^{f/f}$ mice. Pyramidal neurons enriched genes: *Dlg4, Shank1* and *Grin2b*; oligodendrocytes enriched genes: *Mog* and *Sox 10*; microglia enriched genes: *Cx3cr1* and *Cd11b*; astrocytes enriched gene *Aldh1l1* (*$p < 0.05$, **$p < 0.01$, ***$p < 0.001$, *t*-test). E. Bar graph showing the mRNA level of *Igf1r* in input (total mRNA) and CaMKII-TRAP mRNAs from PFC of GFP-L10a$^{f/f}$ mice. F-G. Representative images showing IGF1R (green) expression in pyramidal neurons infected with CaMKII-mCherry-AAV (red) in PFC from adult WT mice. Data are shown as the mean ± SEM.

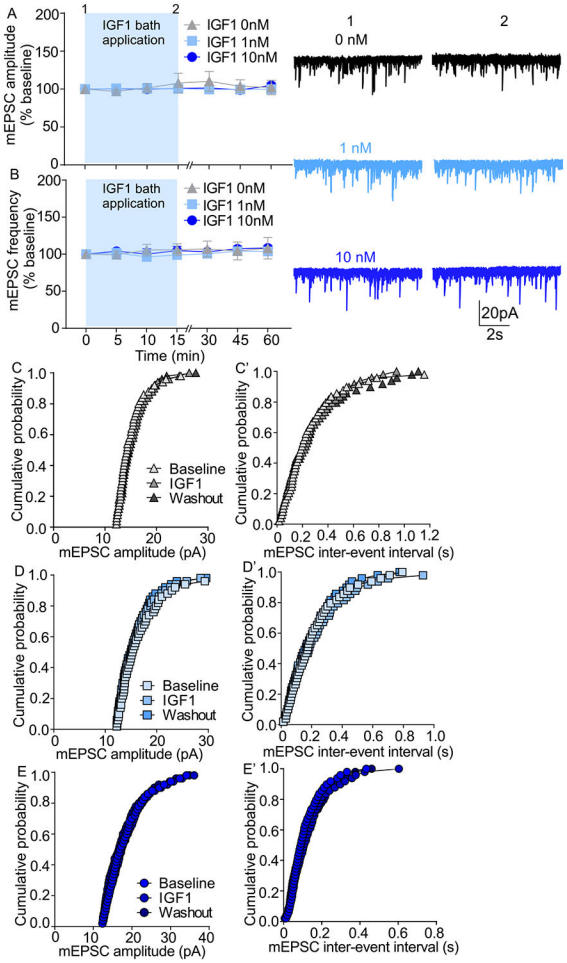

Fig. 2.

IGF1 does not change mEPSC amplitude or frequency in pyramidal neurons from adult PFC. A-B. Average mEPSC amplitude (A) and frequency (B) recorded from PFC layer V pyramidal neurons during bath application of IGF1 (0 nM, 1 nM and 10 nM) and following washout. Right: representative mEPSC traces before and after IGF1 application. C-E'. Cumulative probability distributions of mEPSC amplitude (C–E) and frequency (C′-E′) before (baseline) and after IGF1 bath application (C–C′, 0 nM; D-D′, 1 nM; E-E′, 10 nM) and following washout. Data are shown as the mean ± SEM.

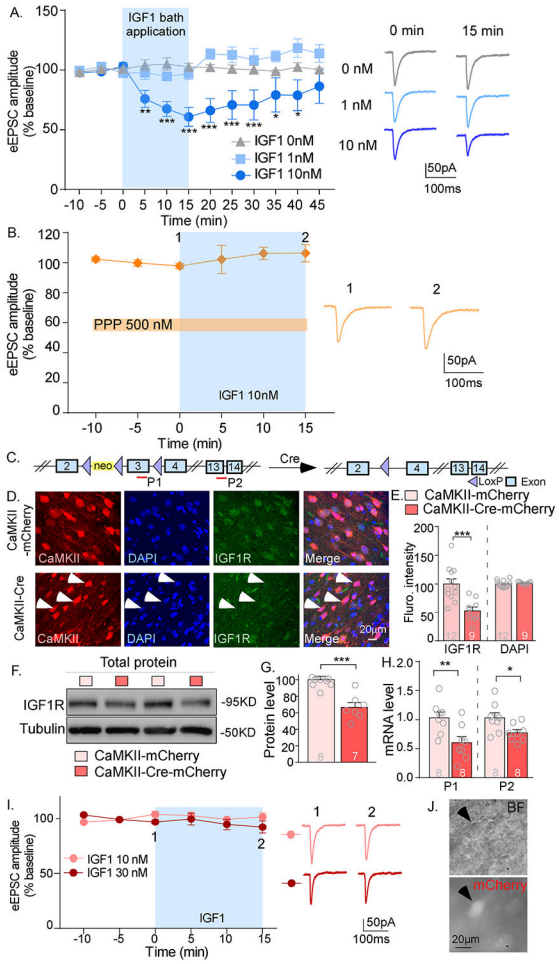

Fig. 3.

IGF1 attenuates eEPSC amplitude in pyramidal neurons from adult PFC via activation of IGF1R. A. Average eEPSC amplitude recorded from PFC layer V pyramidal neurons during baseline (control), bath application of IGF1 (0 nM, 1 nM and 10 nM) and following washout. Right: representative eEPSC traces before and after IGF1 application (*$p < 0.05$, **$p < 0.01$, ***$p < 0.001$, two-way rmANOVA). B. Average eEPSC amplitude recorded from PFC layer V pyramidal neurons before and after 10 nM IGF1 application with the presence of IGF1R antagonist PPP (500 nM). Right: representative eEPSC traces before and after 10 nM IGF1 application with the presence of PPP. C. Schematic of *Igf1r* gene construct and its recombined products with Cre presence. D-E. Representative images (D) and quantification (E) of IGF1R immunofluorescence intensity in the PFC of adult *Igf1R*$^{f/f}$ mice received CaMKII-mCherry-AAV or CaMKII-Cre-mCherry-AAV into PFC. Arrows indicate low IGF1R expression in Cre^{+} cells (***$p < 0.001$, *t*-test). F-G. Representative immunoblots (F) and quantification (G) of IGF1R in the PFC of *Igf1R*$^{f/f}$ mice injected with CaMKII-mCherry-AAV or CaMKII-Cre-mCherry-AAV (***$p < 0.001$, *t*-test). H. *Igf1R* mRNA level detected by primer 1 (P1) and 2 (P2) in the PFC of *Igf1R*$^{f/f}$ mice injected with CaMKII-mCherry-AAV or CaMKII-Cre-mCherry-AAV (*$p < 0.05$, **$p < 0.01$, *t*-test). I. Average eEPSC amplitude before and after 10 nM or 30 nM IGF1 application in PFC slices from *Igf1R*$^{f/f}$ mice injected with CaMKII-Cre-mCherry-AAV into the PFC. Right:

representative eEPSC traces before and after 10 nM IGF1 application. J. Visualization of mCherry^{+} pyramidal neurons in the PFC during recording. Data are shown as the mean ± SEM.

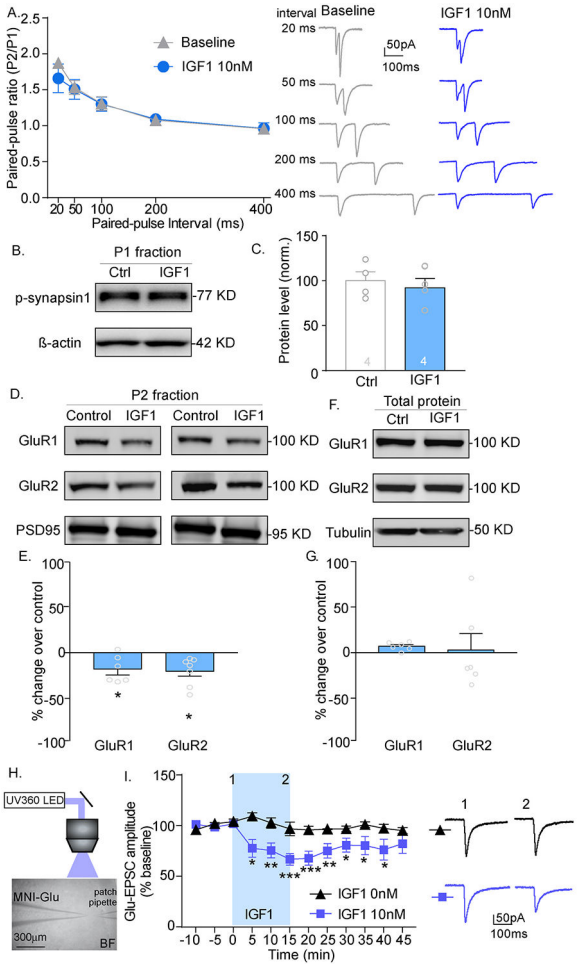

Fig. 4.

IGF1-induced suppression of eEPSC amplitude is related to post-synaptic effect. A. Paired-pulse ratio (PPR) in PFC layer V pyramidal neurons before (baseline) and after 10 nM IGF1 bath application (15 min) at different intervals. Right: representative PPR traces before and after 10 nM IGF1 application. B–C. Representative immunoblots (B) and quantification (C) of p-synapsin I in P1 fraction (cytosolic proteins in synapses) of PFC punches from brain slices treated with or without 10 nM IGF1 (15 min). D-E. Representative immunoblots (D) and quantification (E) of GluR1 and GluR2 in P2 fraction (membrane-associated proteins in synapses) of PFC punches from brain slices treated with or without 10 nM IGF1 (15 min, $*p < 0.05$, *t*-test). F-G. Representative immunoblots (F) and quantification (G) of GluR1 and GluR2 in total protein lysate of PFC punches from brain slices treated with or without 10 nM IGF1 (15 min). H. Schematic of full-field glutamate uncaging approach using UV light (360 nm), and representative image showing the position of pipette delivering 1 mM MNI-caged-L-glutamate (MNI-Glu) and patching pipette. I. Averaged glu-EPSC amplitude recorded from PFC layer V pyramidal neurons during baseline (control), bath application of 0 nM or 10 nM IGF1 and following washout. Right: representative glu-EPSC traces before and after IGF1 application (*p < 0.05, **p < 0.01, ***p < 0.001, two-way rmANOVA). Data are shown as the mean ± SEM.

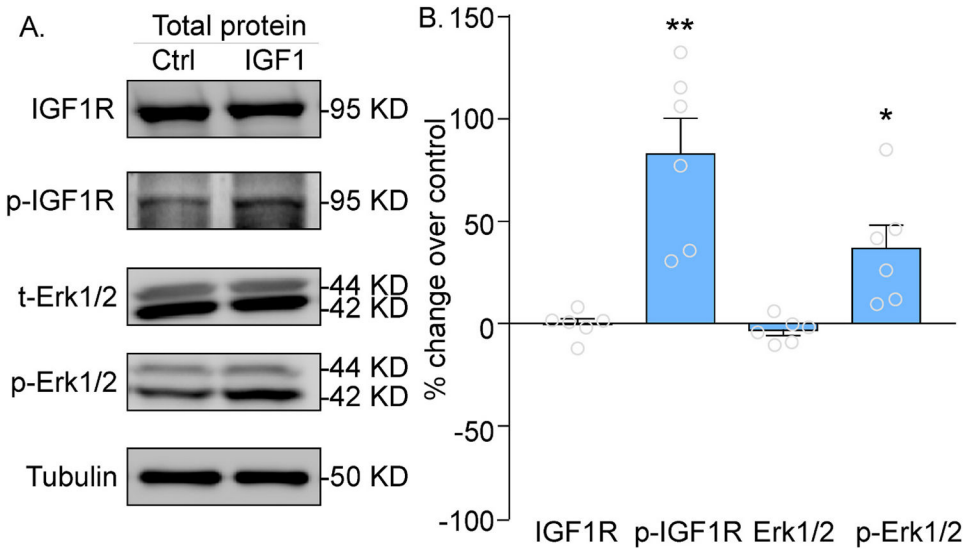

Fig. 5.

IGF1-induced activation of IGF1R is accompanied by activated Erk1/2 signaling pathway. A-B. Representative immunoblots (A) and quantification (B) of IGF1R, p-IGF1R, t-Erk1/2 and p-Erk1/2 in total protein lysate of PFC punches from brain slices treated with or without 10 nM IGF1 (15 min, $*p < 0.05$, $**p < 0.01$, *t*-test). Data are shown as the mean ± SEM.

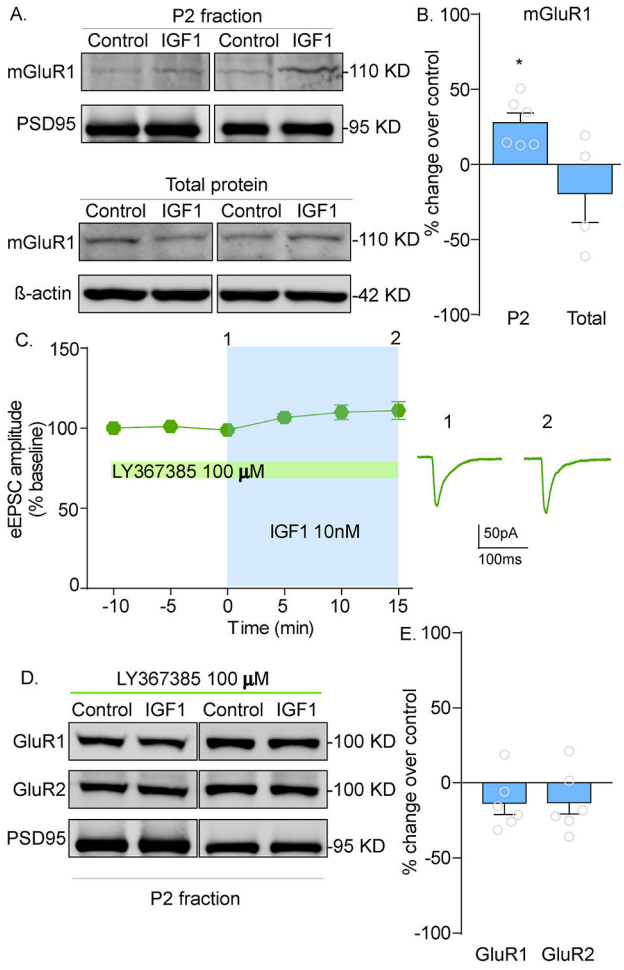

Fig. 6.

IGF1-induced attenuation of eEPSC amplitude is mGluR1 dependent. A-B. Representative immunoblots (A) and quantification (B) of mGluR1 in P2 fraction (top panel) and total protein lysate (bottom panel) of PFC punches from brain slices treated with or without 10 nM IGF1 (15 min, $*p < 0.05$, *t*-test). C. Average eEPSC amplitude recorded from PFC layer V pyramidal neurons before and after IGF1 bath application with the presence of mGluR1 antagonist LY367385 (100 µM). Right: representative eEPSC traces before and after 10 nM IGF1 application with the presence of LY367385. D-E. Representative immunoblots (D) and quantification (E) of GluR1 and GluR2 in P2 fraction (membrane-associated proteins in synapses) of PFC punches from brain slices incubated with or without 10 nM IGF1 (15 min) with the pre-treatment of mGluR1 antagonist LY367385 (100 µM). Data are shown as the mean ± SEM.